

RESEARCH

Open Access



Carboxyl truncation of α -synuclein occurs early and is influenced by human APOE genotype in transgenic mouse models of α -synuclein pathogenesis

Grace M. Lloyd^{1,2}, Brooke Long¹, Stephan Quintin^{1,2}, Zachary A. Sorrentino^{1,2}, Kimberly-Marie M. Gorion^{1,2}, Brach M. Bell^{1,2}, Denise Carrillo¹, Patrick Sullivan⁴, David Borchelt^{1,2,3} and Benoit I. Giasson^{1,2,3*} 

Abstract

Post-translational modifications to the carboxyl (C) terminus domain of α -synuclein can play an important role in promoting the pathologic aggregation of α -synuclein. Various cleavages that diminish this highly charged, proline-rich region can result in exposure of hydrophobic, aggregation-prone regions, thereby accelerating the aggregation kinetics of α -synuclein into misfolded, pathologic forms. C-terminally truncated forms of α -synuclein are abundant in human diseased brains compared to controls, suggesting a role in disease pathogenesis. Factors that alter the homeostatic proteolytic processing of α -synuclein may ultimately tip the balance towards a progressive disease state. Apolipoprotein E (APOE) has been implicated in the acceleration of cognitive impairment in patients with Lewy body diseases. The APOE4 isoform has been found to cause dysregulation in the endosomal–lysosomal pathway, which could result in altered α -synuclein degradation as a potential mechanism for promoting its pathologic misfolding. Herein, we investigate the spatiotemporal accumulation of C-terminally truncated α -synuclein in a seeded and progressive mouse model of synucleinopathy. Furthermore, we study how this process is influenced in the context of mice that are altered to express either the human APOE3 or APOE4 isoforms. We found that specific C-terminal truncation of α -synuclein occurs at early stages of pathogenesis. We also found that proteolytic processing of this domain differs across various brain regions and is influenced by the presence of different human APOE isoforms. Our data demonstrate an early pathogenic role for C-terminally truncated α -synuclein, and highlight the influence of APOE isoforms in modulating its impact.

Keywords Alpha-synuclein, Post-translational modifications, Synucleinopathies, Parkinson's disease, Dementia with Lewy bodies, Multiple system atrophy, Alzheimer's disease with amygdala predominant Lewy bodies, C-terminal truncation, APOE

*Correspondence:

Benoit I. Giasson
bgiasson@ufl.edu

Full list of author information is available at the end of the article



© The Author(s) 2023. **Open Access** This article is licensed under a Creative Commons Attribution 4.0 International License, which permits use, sharing, adaptation, distribution and reproduction in any medium or format, as long as you give appropriate credit to the original author(s) and the source, provide a link to the Creative Commons licence, and indicate if changes were made. The images or other third party material in this article are included in the article's Creative Commons licence, unless indicated otherwise in a credit line to the material. If material is not included in the article's Creative Commons licence and your intended use is not permitted by statutory regulation or exceeds the permitted use, you will need to obtain permission directly from the copyright holder. To view a copy of this licence, visit <http://creativecommons.org/licenses/by/4.0/>. The Creative Commons Public Domain Dedication waiver (<http://creativecommons.org/publicdomain/zero/1.0/>) applies to the data made available in this article, unless otherwise stated in a credit line to the data.

Introduction

Parkinson's disease (PD) is a devastating neurodegenerative disorder, characterized by the slow, progressive loss of motor movement function and control due to degeneration, and eventual death, of dopaminergic neurons in the substantia nigra pars compacta [35]. Molecular investigations into the pathophysiology of PD has revealed the misfolding, aggregation and progressive accumulation of α -synuclein (α Syn) as inclusion pathology, termed Lewy bodies (LBs), to be a major recurrent feature in this disease [5]. Furthermore, this protein has been found to accumulate in many other neurodegenerative diseases, termed synucleinopathies [16]. Common symptoms of synucleinopathies include progressive motor dysfunction, however, cognitive features can be a major component, especially for dementia with Lewy bodies [31, 36]. Recent investigations into synucleinopathies with cognitive features have uncovered curious connections to a major Alzheimer's disease (AD)—associated gene, apolipoprotein E (*APOE*; HGNC:613). Genome-wide association studies (GWAS) and meta-analyses have exposed the $\epsilon 4$ allele variant of the *APOE* gene (*APOE* $\epsilon 4$) as a contributing risk factor for increased rate of cognitive decline, worsened cognitive impairment and/or earlier onset of dementia in synucleinopathies with cognitive features [4, 9, 18, 21, 30, 34, 37–39, 41, 48, 49]. Studies on the role of *APOE* genotype and cognition in PD provide evidence that *APOE* may directly impact the pathological progression of α Syn in PD [9, 11, 22, 48, 49]; subsequently, in vivo investigations have demonstrated an *APOE* $\epsilon 4$ mediated exacerbation of α Syn pathology in murine models of synucleinopathy [9, 52]. Furthermore, protein levels of *APOE* dramatically increase in humans with PD [51], as well as in diseased, transgenic α Syn models with PD-related mutations [14]. These findings confirm a modulatory role for *APOE* in the pathogenesis of α Syn, however, the molecular mechanisms underlying these observations are not well understood.

One possible mechanism by which *APOE* influences α Syn pathogenesis is via the dysregulation of autophagic processes in an isoform-dependent manner. Aberrant proteolysis is a major feature in synucleinopathies and is linked to increased α Syn accumulation [3, 6, 12, 15, 27, 32]. α Syn proteolysis leads to the formation of cytotoxic, partially degraded, α Syn fragments [17], and, importantly, carboxy-terminally truncated forms of α Syn (α Syn Δ C), which are hypothesized to be a key precipitating component of α Syn pathogenesis [2, 25, 28, 44]. In the studies herein, we explored the supposition that α Syn Δ C contributes to α Syn pathogenesis, as well as the effect of *APOE* genotype on this process. Using antibodies specific for α Syn Δ C-103, -114, -122, -125 and -129, which we have recently established, we assessed the extent to

which intramuscular (IM), peripheral seeding with α Syn pre-formed fibrils (PFFs) injection into M83 α Syn transgenic animals resulted in the temporal and spatial pathological formation and distribution of α Syn Δ C species. Furthermore, using M83 transgenic animals altered on either a human *APOE* $\epsilon 3^{+/+}$ or and human *APOE* $\epsilon 4^{+/+}$ background, we investigated the effect of *APOE* genotype on modulating the accumulation of these proteolytically cleaved species.

Materials and methods

Animal research ethics statement

All animal experimental procedures were performed in accordance to University of Florida Institutional Animal Care and Use Committee regulatory policies following approval.

Mouse lines and tissue sources

This study utilized a combination of archival tissues from a previous time course study of Tg(Prnp-SNCA**A53T*) $^{+/-}$, abbreviated hereinafter as TgM83 $^{+/-}$ [45], as well as newly generated animals. For the time course study, tissues from a total of 38 TgM83 $^{+/-}$ animals were included in this study, 33 of which had been injected intramuscularly with mouse α Syn preformed fibrils (PFFs) and 5 were naïve animals (Summarized in Table 1).

M83 mice that co-express humanized *APOE* alleles were newly generated for this study. *APOE* targeted replacement mice with either the homozygous *APOE* $\epsilon 3$ or *APOE* $\epsilon 4$ humanized alleles [23, 46, 47] were obtained from Dr. Patrick Sullivan (Duke University, Durham, NC). TgM83 $^{+/+}$ mice were crossed with *APOE* $\epsilon 3^{+/+}$ or *APOE* $\epsilon 4^{+/+}$ mice to produce the F1 generation; 100% of the offspring were heterozygous for the humanized *APOE* and TgM83 alleles. Pups from the F1 generation were then backcrossed with the respective homozygous humanized *APOE* mice, and screened for mice that are homozygous for the *APOE* $\epsilon 3$ or *APOE* $\epsilon 4$ alleles and positive for the TgM83 allele resulting in *APOE* $\epsilon 3^{+/+}$ /M83 $^{+/-}$ or *APOE* $\epsilon 4^{+/+}$ /M83 $^{+/-}$ mice. Mice were mated with respective *APOE* $\epsilon 3^{+/+}$ or *APOE* $\epsilon 4^{+/+}$ while screening for the TgM83 allele for two additional generation to be used for the studies. Since humanized *APOE* $\epsilon 3^{+/+}$ and *APOE* $\epsilon 4^{+/+}$ mice are on a C57BL/6J background, for comparison, TgM83 $^{+/+}$ mice were mated with non-transgenic (nTg) C57BL/6J mice (Jackson Laboratory) to generate TgM83 $^{+/-}$ that were subsequently maintained in a C57BL/6 J for 3–4 generations. Mice were housed in a stable environment with a 12-h light/dark cycle and access to food and water ad libitum. 51 mice were used in total including: 8 TgM83 $^{+/-}$ mice, all of which were injected with pre-formed fibrils (PFFs) (6F:2M), 24 *APOE* $\epsilon 3^{+/+}$ /M83 $^{+/-}$ mice, 12 (6F:6M) injected with phosphate

Table 1 Summary of animals used in time-course study

Time-course study	
Animal model	TgM83 ^{+/-} (C3H/BL6)
Cohorts	1 m.p.i.; n = 8 (4F:4M) 2 m.p.i.; n = 9 (5F:4M) 3 m.p.i.; n = 8 (4F:4M) Aged until paralysis; n = 8 (5F:3M) naïve; n = 5 (4F:1M)
Type/amount of injection	10 µg of mouse αSyn PFFs in 5 µl PBS (20 µg total); or PBS
Age of injection	2 months
Region of injection	Bilateral injection in gastrocnemius muscle
Age at harvest	1 m.p.i., 2 m.p.i., 3 m.p.i. and at onset of motor impairment
Total n	38

buffered saline (PBS), 12 (6F:6M) injected with PFFs, and 19 APOE ε4^{+/+}/M83^{+/-} mice, 7 (3F:4M) injected with PBS, 12 (6F:6M) injected with PFFs. Mouse data is summarized in Table 2.

αSyn fibril preparation

For the TgM83^{+/-} study with varying APOE isoforms, human PFFs generation was prepared as follows: recombinant human αSyn was expressed in *E. coli* then purified using size exclusion and ion exchange chromatography as previously described [42]. Human αSyn protein (5 mg/ml in sterile phosphate buffered saline (PBS)) was incubated at 37 °C with constant shaking at 1050 RPM (Thermomixer R, Eppendorf) for 5 days to induce fibrillization. Fibril formation was monitored by K114 [(trans, trans)-1-bromo-2,5-bis-(4-hydroxy) styrylbenzene] fluorometry as previously described [7]. Fibrils were diluted to 2 mg/ml in sterile PBS and fragmented via water bath sonication at 40 kHz for 1 h at RT, prior to injection, as previously described [43].

Gastrocnemius injection and survival analysis

For the time-course study, intramuscular (IM) injection and tissue processing for animals were previously described [45]. Briefly, at 2 months of age, mice were deeply anesthetized with isoflurane (1–5%) inhalation, then bilaterally injected in the gastrocnemius muscles, with 10 µg of mouse αSyn PFFs in 5 µl of sterile PBS. For the APOE/M83^{+/-} study, mice were aged for 2 months, then injected in the right gastrocnemius with 5 µg of human PFFs (1 µg/µl) or sterile PBS. Following inoculation, mice were regularly assessed for motor deficits. For both studies, the survival end point was motor impairment/paralysis, upon which the animals were euthanized. For the APOE/M83^{+/-} study, mice were aged until the onset of motor symptoms or until the pre-determined study end point at 185 days post-injection.

Development and validation of antibodies specific various forms of αSynΔC

Monoclonal antibodies specific for αSyn carboxy (C)-terminally truncated at residues 103, 114, 122, 125 or 129 [20, 40] (see Table 3) were previously described.

Table 2 Summary of animals used in APOE genotype study

APOE genotype study			
Animal model	TgM83 ^{+/-} (BL6)	APOE ε3 ^{+/+} /TgM83 ^{+/-}	APOE ε4 ^{+/+} /TgM83 ^{+/-}
Cohorts	PFF-injected; n = 8 (6F:2M)	PFF injected; n = 12 (6F:6M) PBS injected; n = 12 (6F:6M)	PFF injected; n = 12 (6F:6M) PBS injected; n = 7 (3F:4M)
Type/amount of injection	5 µg of human αSyn PFFs in 5 µl PBS; or PBS		
Age of injection	2 months		
Region of injection	Unilateral injection in right gastrocnemius muscle		
Age at harvest	8 months post-injection unless motor impaired		
Total n	51		

Table 3 Summary of antibodies and antigen retrieval methods used in study

Key resources table					
Primary antibodies	Identifier	Specificity	Antigen retrieval for IHC	Source	References
Anti- α Syn pS129, Mouse	81A RRID: AB_2819037	α -syn at pSer129	Water w/0.05% Tween, heat bath	B. Giasson University of Florida College of Medicine; Florida; USA	[50]
p62/ sequestresome-1, Rabbit	p62	Sequestresome1	Water w/0.05% Tween, heat bath	ProteinTech, Rosemont, IL	[24]
Anti- α Syn, Mouse	2H6	α Syn (2–21)	Water w/0.05% Tween, heat bath	B. Giasson University of Florida College of Medicine; Florida; USA	[10]
Anti- α Syn, Mouse	3H19	α Syn (110–119)	DAKO Target Retrieval Solution, heat bath/70% formic acid	B. Giasson University of Florida College of Medicine; Florida; USA	[29]
Anti- α Syn cleaved at 103, Mouse	2G5	α Syn (x-103)	Formalin incubation/DAKO Target Retrieval Solution, heat bath/70% formic acid	B. Giasson University of Florida College of Medicine; Florida; USA	[20]
Anti- α Syn cleaved at 114, Mouse	1A2	α Syn (x-114)	DAKO Target Retrieval Solution, heat bath/70% formic acid	B. Giasson University of Florida College of Medicine; Florida; USA	[40]
Anti- α Syn cleaved at 122, Mouse	10A4	α Syn (x-122)	DAKO Target Retrieval Solution, heat bath/70% formic acid	B. Giasson University of Florida College of Medicine; Florida; USA	[20]
Anti- α Syn cleaved at 125, Mouse	5C1	α Syn (x-125)	DAKO Target Retrieval Solution, heat bath/70% formic acid	B. Giasson University of Florida College of Medicine; Florida; USA	[20]
Anti- α Syn cleaved at 129, Mouse	2G7	α Syn (x-129)	DAKO Target Retrieval Solution, heat bath/70% formic acid	B. Giasson University of Florida College of Medicine; Florida; USA	[20]

Tissue processing and immunohistochemical analysis

For immunohistochemistry (IHC) studies, mice were euthanized with CO₂, and perfused with a heparin/PBS solution, as previously described [45]. Briefly, brains and spinal cords of mice were harvested and fixed in 70% EtOH/150 mM NaCl, paraffin embedded, and coronally cut into 5 μ m sections, as previously described [45]. Immunostaining was performed using established methods [13]. Briefly, tissue sections were rehydrated with xylenes and graded, 100–70% ethanol steps followed with heat-induced epitope retrieval (HIER) in a steam bath for 60 min using retrieval method indicated in Table 3. After antigen retrieval, sections were washed in running deionized H₂O for 15 min. For 3H19 antibody and all of the α Syn C-truncation specific antibodies, sections were then treated with 70% formic acid for 10 min, then rinsed in running deionized H₂O for 15 min. Endogenous peroxidase was quenched by incubating sections in 1.5% hydrogen peroxide/0.005% Triton-X-100 diluted in PBS, pH 7.4 (Invitrogen) for 15–20 min. For antibody 2G5, Triton-X-100 was omitted from this step. Sections were then rinsed in running deionized H₂O for 15 min. Slides were washed 3 times for 5 min in 0.1 M Tris, pH 7.6, or Tris buffered saline (TBS; 50 mM Tris, pH 7.5, 150 mM NaCl) (for

1A2 only), then blocked for 10 min in 2% fetal bovine serum (FBS)/0.1 M Tris solution or 5% milk/TBS (1A2 only). Sections were incubated with primary antibodies diluted in blocking solution, if required, and stored overnight in 4°. After overnight incubation, primary antibody was removed from slides with a quick rinse, then incubated with agitation for 5 min in 0.1M Tris or TBS (for 1A2 only), 3 times. Tissue sections were incubated for 1 h with biotinylated secondary IgG (Vector Laboratories; Burlingame, CA) in 0.1M Tris, pH 7.6/2% FBS or 5% milk/TBS (for 1A2 only) at 1:3000 at RT. For 3H19 antibody and all of the α Syn C-truncation specific antibodies, ImmPRESS polymer secondary antibody (Vector Laboratories; Burlingame, CA) was diluted in a 1:10 ratio with the standard secondary antibody solution described above. Secondary antibody was rinsed 3 times with 0.1M Tris, or TBS (for 1A2 only), for 5 min each. Sections were then incubated with an avidin–biotin complex (ABC) solution (Vectastain ABC Elite kit; Vector Laboratories, Burlingame, CA) for 1 h at RT, then rinsed again, 3 times, with 0.1M Tris, or TBS (for 1A2 only), for 5 min each. Sections were developed using chromogen 3,3'-diaminobenzidine (DAB kit; KPL, Gaithersburg, MD), rinsed for 15 min in running tap water, then counterstained using hematoxylin

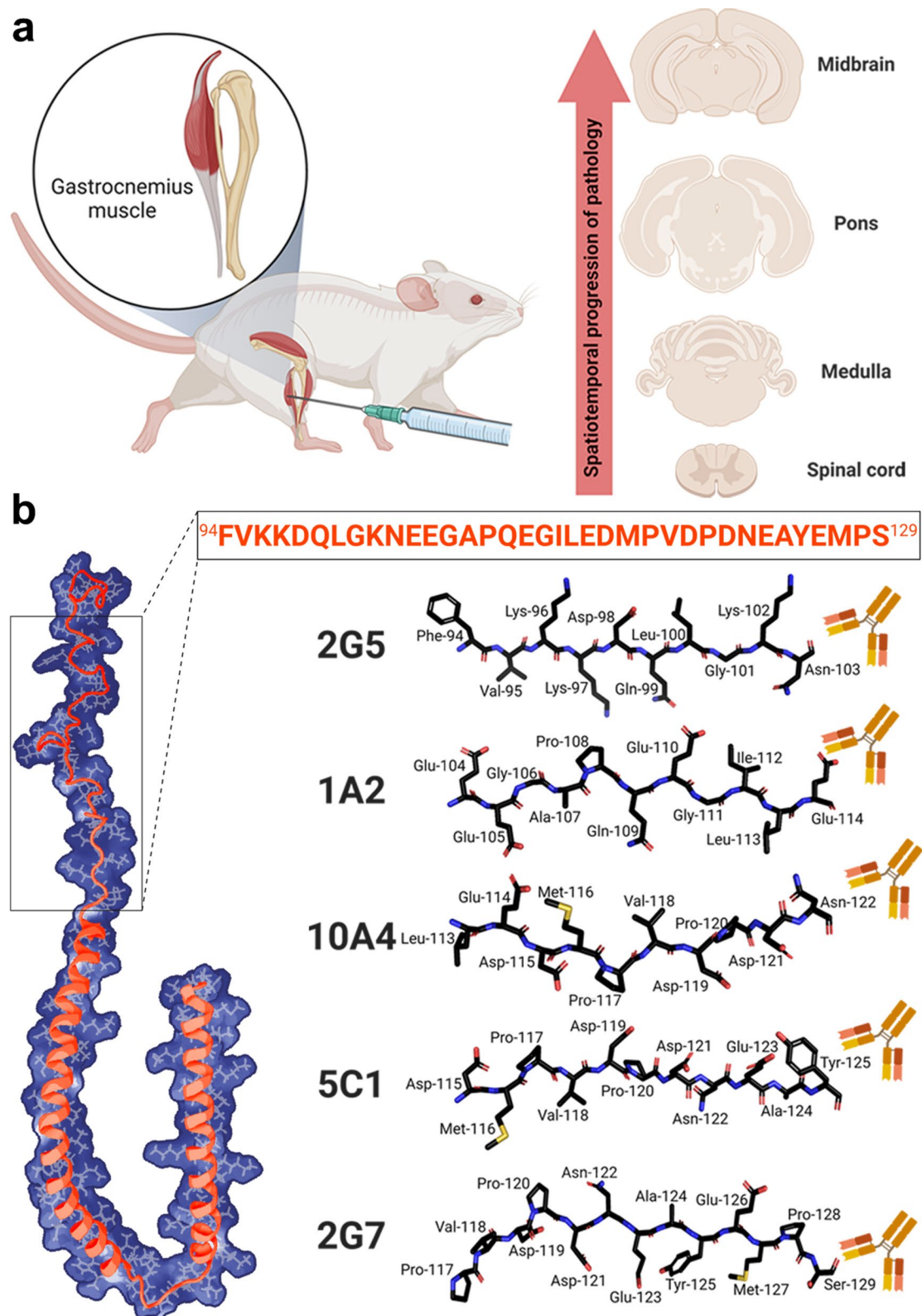


Fig. 1 Schematics of experimental designs assessing the spatiotemporal progression of aSyn inclusion pathology including various aSynΔC forms. **(a)** Representative illustration of experimental design showing IM injection of PFFs and theorized route of spatiotemporal pathological propagation of aSyn type prion transmission. **(b)** Stick diagrams of peptide sequences used to generate aSynΔC specific aSyn antibodies. Antibodies are not drawn to scale. Structural model is based on PDB accession 1XQ8. Created with Biorender.com

(Sigma Aldrich, St. Louis, MO). Summary of antibodies used and corresponding retrieval methods are summarized in Table 3.

Semi-quantification and digital analysis of pathology

All IHC sections were digitally scanned using an Aperio ScanScope CS instrument (40× magnification; Aperio Technologies Inc., Vista, CA, USA), and images of representative areas of pathology were captured using the ImageScope software (40× magnification; Aperio Technologies Inc. Vista, CA, USA). Tissue sections were manually scored for α Syn pathology on a scale of 0 (no pathology) to 3 (highest pathology) by three independent raters using the Allen Brain Atlas to define regions (Allen Reference Atlas—Mouse Brain [brain atlas]. Available from atlas.brain-map.org) [1, 8, 19, 26, 33]. Morphological descriptions were classified using categories defined previously [29]. Representative images were corrected for color/hue values; brightness/contrast adjustments were applied identically on captured images within each figure using Adobe Photoshop CS3 (Adobe Systems, San Jose, CA, USA). All raw files are available upon request.

Statistical analysis

Experiments were analyzed using parametric statistical tests described in detail in the figure legends. No animals were excluded from analysis. Data was tested for normality using D'Agostino-Pearson omnibus test. Statistical analysis was performed using Prism software (GraphPad Software, San Diego, CA, USA) and detailed in figure legends. For time-course experiments, results were analyzed using 2-way ANOVA and corrected for multiple comparisons using the Tukey test. Kaplan–Meier curves of motor phenotype development were compared using Log-rank (Mantel–Cox). Column analysis of data with more than 2 groups were analyzed by 1-way ANOVA corrected for multiple comparisons using Tukey's test. For 2-way ANOVAs, simple effects comparing the mean between groups was reported (detailed in figures). Graphs depicting correlations were computed using Pearson's correlation coefficients (Pearson r and two-tailed p -value annotated on graphs) and shown with a simple linear regression line with 95% confidence bands of the best-fit line. P values were multiplicity adjusted,

family-wise significance was set at 0.05 and data are presented as mean \pm SEM.

Results

Immunohistopathological analysis of PFF intramuscularly injected TgM83^{+/-} mice using novel α Syn Δ C specific antibodies

To assess the spatiotemporal progression of α Syn Δ C pathology, we analyzed archival tissues from a cohort of animals that have previously published [45]. In that study, TgM83^{+/-} mice were injected bilaterally in the gastrocnemius muscle with mouse PFFs, or PBS at 2 months of age. PFF-injected mice were harvested at 1-, 2-, or 3- months post injection (m.p.i.), or upon paralysis; naïve mice control mice were harvested at the same timepoints (Fig. 1a).

We previously reported that spinal motor neuron degeneration in TgM83^{+/-} mice, begins at approximately 2 months post-IM injection even though pSer129 positive α Syn pathology is limited [45]. We also found that pSer129 positivity increased over time and throughout neuroanatomically connected regions, in PFF-injected mice, while naïve mice display no α Syn pathology [45]. In this study, IHC analysis was performed with α Syn Δ C specific antibodies, generated and characterized previously, [20, 40] targeting α Syn Δ C truncated at residues 103, 114, 122, 125, and 129 (Fig. 1b). We investigated whether α Syn Δ C positivity is detected in regions distal to injection site, and whether burden of α Syn Δ C positive inclusions increase with age. Similar to staining for pSer129, α Syn Δ C positivity was not detected in naïve mice [45] (data not shown).

α Syn Δ C forms of α Syn are detected in the spinal cord at 2-months post IM injection of PFFs and increase temporally

Following IM injection of PFFs in TgM83^{+/-} mice, α Syn inclusion pathology was not detected at 1 m.p.i. as it is first detected at 2 m.p.i. in the intermediate and ventral regions of the spinal cord (Fig. 2) [45]. Therefore, to investigate the earliest occurrence of α Syn Δ C pathology, we probed spinal tissue with antibodies targeting pSer129 and α Syn Δ C-103, -114, -122, -125 and -129. Three different C-terminally truncated forms of α Syn, α Syn Δ C-103 (2G5), α Syn Δ C-122 (10A4), and α Syn Δ C-125 (5C1), were detectable in inclusions by 2 m.p.i. (Fig. 2). 2G5

(See figure on next page.)

Fig. 2 Progressive accumulation of α Syn pathology and α Syn Δ C forms in the spine of TgM83^{+/-} mice following peripheral intramuscular administration of PFFs. **(a)** Representative IHC images comparing α Syn pathological deposition in TgM83^{+/-} mice at 1-, 2-, or 3- months post IM injection or terminal stage. Antibodies specific for α Syn phosphorylated at Ser129 (81A) and α Syn Δ C at residues 103 (2G5), 114 (1A2), 122 (10A4), 125 (5C1) and 129 (2G7) were used for IHC, as indicated. Sections were counterstained with hematoxylin. Scale bar for high magnification images = 150 μ m; for inset = 15 μ m. **(b)** Semi-quantification of antibody immunoreactivity for α Syn inclusion pathology. Data expressed as mean \pm SEM. Results were analyzed using 2-way ANOVA and corrected for multiple comparisons using Tukey's test. $n = 8$ (4F:4M); 9 (5F:4M); 8 (4F:4M); 8 (5F:3M). * $p < 0.05$; ** $p < 0.01$; *** $p < 0.001$; **** $p < 0.0001$

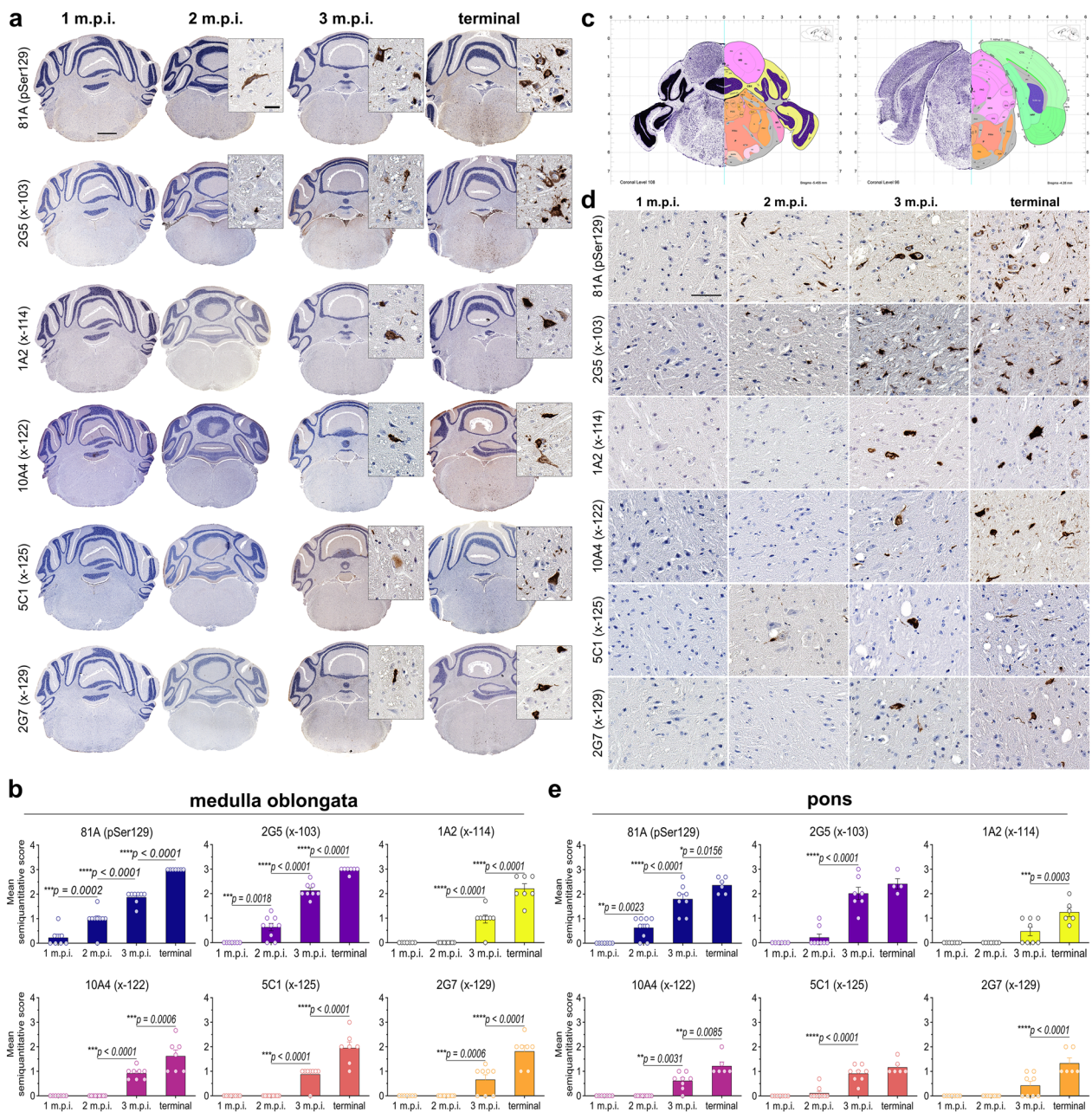


Fig. 3 Detection of α Syn Δ C truncated at residues 103 and 125 in the hindbrain of TgM83^{+/-} mice 2 months after peripheral intramuscular PFF inoculation. Representative IHC images and semiquantitative analysis comparing pathological α Syn deposition in TgM83^{+/-} mice at 1-, 2-, 3- months post IM injection or terminal stage in **(a, b)** the medulla and **(c–e)** the pons. Antibodies specific for α Syn phosphorylated at Ser129 (81A) and α Syn Δ C truncated at residues 103 (2G5), 114 (1A2), 122 (10A4), 125 (5C1) and 129 (2G7) were used for IHC, as indicated. Sections were counterstained with hematoxylin. **c** Nissl (left) and anatomical annotations (right) of coronal section panels from the Allen reference atlas of the adult mouse brain, pons regions analyzed in study are annotated in salmon. Scale bar = 1 mm for low magnitude image and 30 μ m for inset in **(a)** and 60 μ m in **(d)**. Data represents mean \pm SEM. Results were analyzed using 2-way ANOVA and corrected for multiple comparisons using Tukey's test. n = 8 (4F:4M); 9 (5F:4M); 8 (4F:4M); 8 (5F:3M). * p < 0.05; ** p < 0.01; *** p < 0.001; **** p < 0.0001

(α Syn Δ C-103) positive inclusions were found in the anterior horn and intermediate region (Additional file 1: Fig. S1), predominantly as smaller, perinuclear aggregates in glial cells and punctate processes in the neuropil

(Fig. 2a). 10A4 (α Syn Δ C-122) positive inclusions were found in the anterior horn, 5C1 (α Syn Δ C-125) positive inclusions were found in the lateral anterior horn and intermediate region, and 81A (pSer129) positive

inclusions were detected in the anterior and intermediate regions (Additional file 1: Fig. S1) (Fig. 2a). 10A4, 5C1 and 81A positive inclusions shared morphological characteristics, appearing as neuritic processes within the neuropil. By 3 m.p.i., all α Syn Δ C-specific antibodies detected positive inclusions in the spine, and by terminal endpoint, positive α Syn pathology was detected in both dorsal and ventral regions by all antibodies (Additional file 1: Fig. S1), and these inclusions were larger in size (Fig. 2a). Temporal analysis of 81A and 5C1 positive pathology revealed a linear increase between 2 m.p.i. and terminal endpoint (Fig. 2b). Comparatively, 2G5 pathology was relatively low at 2 m.p.i., but increased greatly in abundance by 3 m.p.i. (Fig. 2b). 1A2 and 2G7 reactive pathology was moderate at 3 m.p.i. and approximately doubled between 3 m.p.i. and end stage (Fig. 2b). 10A4 pathology was moderate at 2 m.p.i., displayed a modest increase at 3 m.p.i., and nearly doubled by terminal endpoint (Fig. 2b). Overall, by terminal endpoint, 2G7

(x-129) immunoreactivity revealed the lowest burden of inclusions, while 2G5 (x-103) staining had the highest (Fig. 2b).

α Syn Δ C-103 and α Syn Δ C-125 positive pathology detected at 2 m.p.i. in hindbrain

In order to determine whether the temporal pattern of α Syn Δ C-positive inclusions continues in regions increasingly distal to the injection site, pathology in the hindbrain regions were assessed. In the medulla, the only form of C-terminally truncated α Syn detected at 2 m.p.i. was α Syn Δ C-103 with antibody 2G5, however, all of α Syn C-truncation epitopes were detected at 3 m.p.i. (Fig. 3a–b). By the terminal endpoint, 2G5 immunoreactive pathology was extensive and widespread in the medulla, including in the reticular formation and lateral vestibular nuclei (LAV) (Fig. 3a). 2G5 inclusions were of distinct morphology, appearing as perinuclear and intranuclear dots, web-like, and ringed cell body inclusions, lightning,

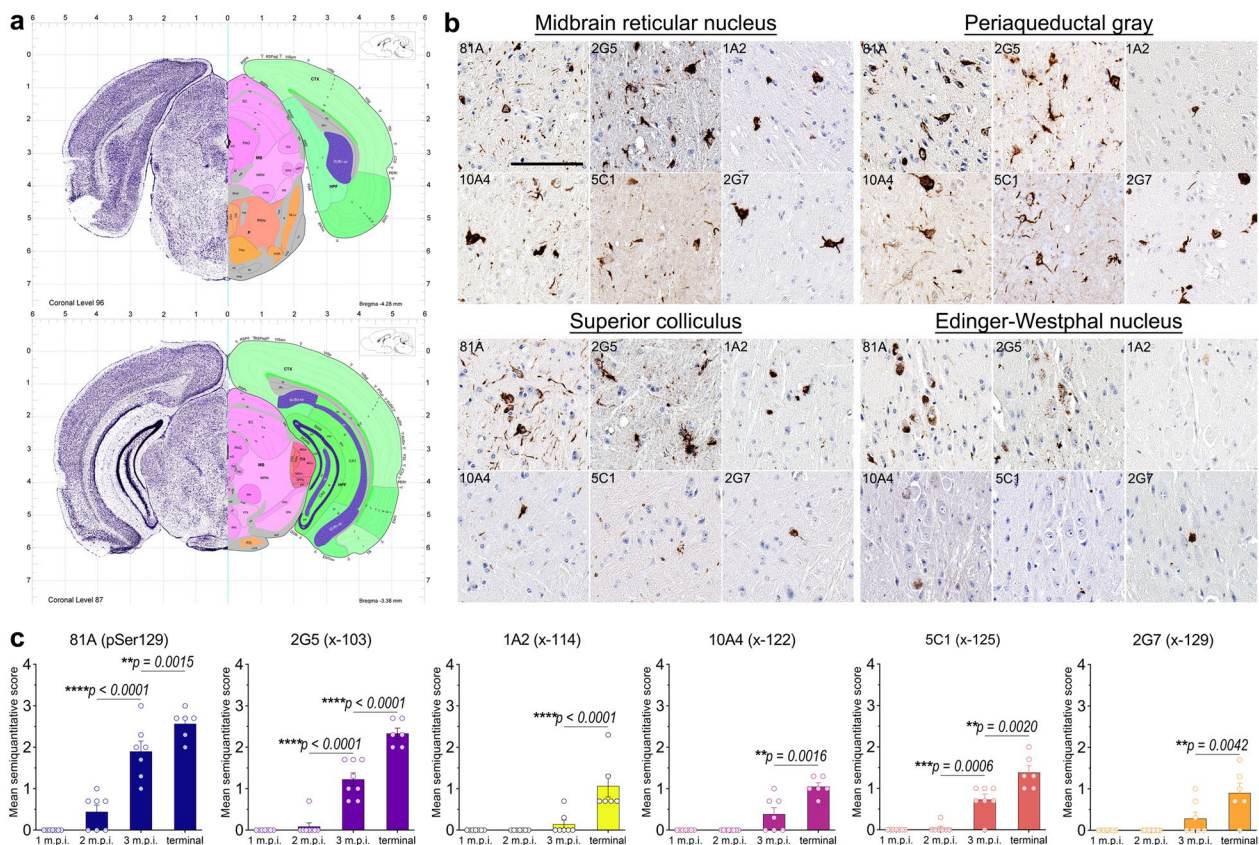


Fig. 4 Accumulation of α Syn Δ C in the midbrain of end stage TgM83^{+/-} mice after peripheral intramuscular PFF induction. **(a)** Nissl (left) and anatomical annotations (right) of coronal section panels from the Allen reference atlas of the adult mouse brain, midbrain regions analyzed in study are annotated in pink. **(b, c)** Representative IHC images and semi-quantification of antibody immunoreactivity comparing the pathological α Syn deposition of TgM83^{+/-} mice at end stage. Antibodies specific for α Syn phosphorylated at Ser129 (81A) and α Syn Δ C truncated at 103 (2G5), 114 (1A2), 122 (10A4), 125 (5C1) and 129 (2G7) were used for IHC, as indicated. Sections were counterstained with hematoxylin. Scale bar = 100 μ m. Data expressed as mean \pm SEM. Results were analyzed using 2-way ANOVA and corrected for multiple comparisons using Tukey's test. n = 8 (4F:4M); 9 (5F:4M); 8 (4F:4M); 8 (5F:3M). *p < 0.05; **p < 0.01; ***p < 0.001; ****p < 0.0001

corkscrew, and beaded neurites, axonal spheroids and dot-like neuropil (Fig. 3a). Of note, 2G5 inclusion pathology was rare or not found in the interpolar part of the spinal nucleus of the trigeminal (SPVI), inferior olivary complex (IO), or nucleus prepositus (PRP). By the terminal endpoint, medullary 1A2 immunoreactive pathology was regionally constrained, primarily to the gigantocellular reticular nucleus (GRN), the lateral paragigantocellular reticular nucleus (PGRNI), the ventral medullary reticular nucleus (MDRNv), and the magnocellular reticular nucleus (MARN), and rarely in the LAV. (Fig. 3a). By terminal endpoint, medullary 10A4 positive pathology was restricted to the MDRNv, GRN, MARN, PGRNI, the hypoglossal nucleus (cranial nerve (CN) XII), the magnocellular part of the lateral reticular nucleus (LRNm), oral part of the spinal nucleus of the trigeminal (SPVO), spinal vestibular nucleus (SPIV), intermediate reticular nucleus (IRN) and rarely in the LAV, as distorted nucleus, LB-like, flame-shaped inclusions, beaded and corkscrew neurites, dot-like neuropil and neuropil threads (Fig. 3a). By terminal endpoint, medullary 5C1 positive pathology was typically detected in the IRN, MDRNv, nucleus of the solitary tract (NTS), superior vestibular nucleus (SUV), CN XII, dorsal motor nucleus of the vagus nerve (DMX), LRNm, PRP, medial vestibular nucleus (MV), SPIV, SPVI, GRN, IRN, PGRNI and LAV as ringed, LB-like, flame-shaped inclusions, beaded, swollen and corkscrew neurites, dot-like neuropil, and neuropil threads (Fig. 3a). By terminal endpoint, medullary 2G7 positive pathology was detected in the GRN, PGRNI, IRN, MDRNv, LAV and LRNm, as distorted nucleus, swollen neurites, flame-shaped, LB-like and ringed inclusions (Fig. 3a). The pattern of increase in pathological positivity over time in the medullary region was different from that observed in the spinal cord. While the spinal cord showed a more sigmoidal increase in pathological positivity over time, the medullary region displayed a gradual, steady escalation in all forms of α Syn positive pathology at each time point (Fig. 3b). This suggests that the accumulation of pathological positivity in the medulla is more consistent over time compared to the spinal cord, which shows a more variable pattern of accumulation.

To analyze regions within the pons for C-terminally truncated forms of α Syn, we immunostained regions illustrated in the annotated reference in Fig. 3c. Along with pSer129 positive pathology, 2G5 and 5C1 were also detected at 2 m.p.i. (Fig. 3d–e). Similar to the pattern revealed in the medulla, all forms of probed C-terminally truncated α Syn were detected at 3 m.p.i. in the pons (Fig. 3d–e). By the terminal endpoint, pontine 2G5 reactive pathology was widespread and appeared as perinuclear dots, LB-like inclusions, axonal spheroids, neuropil threads and dot-like neuropil (Fig. 3d). By the

terminal endpoint, pontine 1A2 pathology was moderate and restricted to the pontine reticular nucleus (PRN). 1A2 positive morphology consisted of flame-shaped, globose, dot-like neuropil, neuropil threads, swollen and corkscrew neurites (Fig. 3d). By the terminal endpoint, pontine 10A4 pathology was moderate and limited to the PRN and the nucleus of the lateral lemniscus (NLL). 10A4 positive morphology consisted of distorted nucleus, LB-like, flame-shaped, ringed, and globose inclusions, dot-like neuropil and neuropil threads (Fig. 3d). By the terminal endpoint, pontine 5C1 pathology was moderate and widespread throughout the pons. 5C1 positive inclusions presented as flame-shaped, swollen and corkscrew neurites, dot-like neuropil and neuropil threads (Fig. 3d). By the terminal endpoint, pontine 2G7 pathology was moderate and restricted to the PRN as distorted nucleus, swollen neurites, flame-shaped, globose and ringed inclusions (Fig. 3d). In this region, the rate of pSer129 positive pathology increased steadily across each timepoint, a trend that was roughly recapitulated by 1A2 (α Syn Δ C-114), 10A4 (α Syn Δ C-122) and 2G7 (α Syn Δ C-129) positive pathology (Fig. 3e). In contrast, 2G5 (α Syn Δ C-103) and 5C1 (α Syn Δ C-125) positive pathology revealed a more sigmoidal pattern of accumulation over time, wherein a significant spike in immunostaining occurred between 2 and 3 m.p.i., and no significant change in pathology was detected by end stage (Fig. 3e).

α Syn Δ C positive inclusions detected in neuroanatomically connected regions distal to injection site by end stage in α Syn mice

To determine whether α Syn Δ C positive inclusions occurred in more distal anatomically connected regions relation to the site of injection, tissue from the midbrain was probed, indicated in pink in the annotated reference in Fig. 4a, of IM PFF-injected TgM83^{+/-} mice with antibodies targeting pSer129 and α Syn Δ C-103, -114, -122, -125 and -129. At end stage, all forms of C-terminally truncated α Syn investigated in this study were detected in the midbrain (Fig. 4b–c). Analysis of the midbrain reticular nucleus (MRN), periaqueductal gray (PAG), superior colliculus (SCs) and Edinger Westphal nucleus (EW), regions densely populated with pSer129 positive pathology, revealed dramatic heterogeneity in the type of α Syn Δ C inclusions detected (Fig. 4b). The MRN was highest in 2G5 pathology and moderate in 1A2, 10A4, 5C1 and 2G7 pathology (Fig. 4b). The PAG was high in 2G5, 10A4, 5C1 and 2G7 pathology, and low in 1A2 pathology (Fig. 4b). The SCs was high in 2G5 pathology, moderate in 1A2 pathology, and low in 10A4, 5C1 and 2G7 pathology (Fig. 4b). The EW nucleus was high in 2G5 pathology and low in 1A2, 10A4, 5C1 and 2G7 pathology

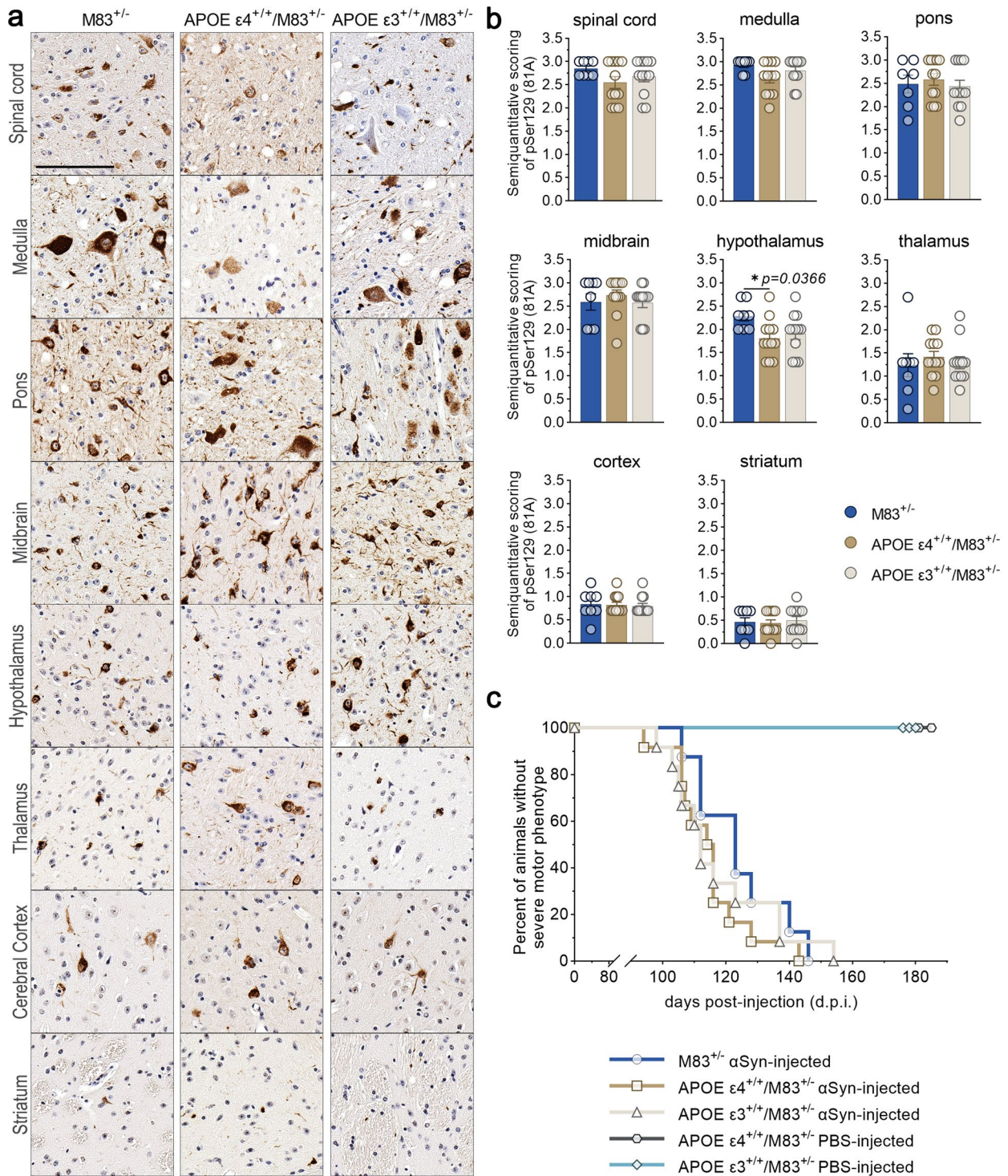


Fig. 5 CNS accumulation of αSyn inclusion pathology in APOE ε4^{+/-}/M83^{+/-} and APOE ε3^{+/-}/M83^{+/-} mice after intramuscular inoculation with PFFs. **(a)** Representative images of immunostaining with an antibody specific for αSyn phosphorylated at serine 129 (81A). Brains and spinal cord from APOE ε3^{+/-}/M83^{+/-} and APOE ε4^{+/-}/M83^{+/-} mice were assessed for relative pathological burden in M83^{+/-} mice. Scale bar = 100 μm. **(b)** Semi-quantification of 81A (pSer129) immunoreactivity in the spinal cord, medulla, pons, midbrain, hypothalamus, thalamus, cortex and striatum of PFF-injected M83^{+/-}, APOE ε4^{+/-}/M83^{+/-} and APOE ε3^{+/-}/M83^{+/-} mice were scored by 3 independent observers. Results were analyzed using 1-way ANOVA and corrected for multiple comparisons using Tukey’s test. Data represents means ± SEM **p* < 0.05; ***p* < 0.01; ****p* < 0.001; *****p* < 0.0001. **(c)** Kaplan–Meier analysis of motor phenotype development in PFF-injected M83^{+/-} (n = 8; median survival, 123 days after injection), APOE ε3^{+/-}/M83^{+/-} (n = 12; median survival, 112 days after injection), and APOE ε4^{+/-}/M83^{+/-} mice (n = 12; median survival, 115 days after injection) see Table 2. Overall Log-rank (Mantel–Cox) *p* = 0.4904

(Fig. 4b). Across the measured timepoints, pSer129 pathology in the pons exhibited a pattern of gradational increase that was congruent for α Syn Δ C-positive pathology (Fig. 4c).

Humanized APOE/M83^{+/-} mice develop mature α Syn inclusion pathology after intramuscular inoculation with PFFs

To investigate the effect of human ApoE isoforms on α Syn Δ C positive pathology, we generated mouse models of synucleinopathy with the background of different human APOE genotypes, by backcrossing the offspring of M83^{+/+} mice and homozygous humanized APOE ϵ 4 or ϵ 3 mice with M83^{+/-} mice for at least 2 generations to APOE ϵ 4^{+/+}/M83^{+/-} and APOE ϵ 3^{+/+}/M83^{+/-} mice (see Materials and Methods). Since humanized APOE mice are on a BL6 background, M83^{+/-} on a BL6 background were also generated for comparison. At 2 months of age, these mice were unilaterally IM injected with human α Syn PFFs. The mice were aged until the onset of fatal motor symptoms, whereupon the brains and spine were collected for IHC analysis.

To determine the profile of pathologic α Syn in these mice, brains and spinal cords from APOE ϵ 3^{+/+}/M83^{+/-} and APOE ϵ 4^{+/+}/M83^{+/-} mice injected with PFFs were assessed for markers of mature α Syn inclusion pathology using antibodies directed towards pSer129 (81A), as a measure of disease-associated α Syn, α Syn at the N-terminus (2H6) and C-terminus (3H19), as well as sequestrase1 (p62). M83^{+/-}, APOE ϵ 4^{+/+}/M83^{+/-} and APOE ϵ 3^{+/+}/M83^{+/-} mice showed robust and extensive, widespread α Syn pathology at end stage (Fig. 5a, Additional file 1: Fig. S2). APOE ϵ 3^{+/+}/M83^{+/-} and APOE ϵ 4^{+/+}/M83^{+/-} mice injected with PBS did not develop α Syn pathology (Additional file 1: Fig. S3). Semi-quantification of 81A pathology revealed a significantly lower level of hypothalamic inclusions in APOE ϵ 4^{+/+}/M83^{+/-} mice compared to M83^{+/-} mice (Fig. 5b), however, all other regions were relatively equal. Analysis of the onset of a motor phenotype revealed no difference between PFF-injected M83^{+/-} mice (n=8; median survival, 123 days after injection), APOE ϵ 3^{+/+}/M83^{+/-} (n=12; median survival, 112 days after injection), or APOE ϵ 4^{+/+}/M83^{+/-} mice (n=12; median survival, 115 days after injection) (Fig. 5c).

Regionally dynamic α Syn Δ C immunoreactive pathology is differentially regulated by APOE genotype

In order to compare the overall burden of α Syn Δ C positive inclusions, IHC analysis was performed using antibodies targeted towards α Syn C-terminally truncated at residue 103, 114, 122, 125, and 129. Regions within the spine and brain, ranging in distance to the injection site including the spinal cord, medulla, pons, midbrain, hypothalamus, thalamus, cortex and striatum were analyzed. Immunostained sections were evaluated via semi-quantitative analysis by 3 independent observers and averaged score were normalized to 81A (Fig. 6). The data for all the α Syn Δ C antibodies, regions analyzed and genotypes are shown in Fig. 6 for easier direct comparison. Our data revealed that α Syn Δ C immunoreactivity was regionally dynamic, and that this was altered based on APOE genotype. This was analyzed in greater detail for each α Syn Δ C antibody. α Syn Δ C-103 (2G5) immunoreactivity was higher in the spine, hindbrain and midbrain for all cohorts compared to forebrain regions (Fig. 7a). For regions that displayed genotype-specific differences such as the spinal cord, pons and cortex, we performed additional statistical analyses (Fig. 7b–c). In the spine, both APOE ϵ 3^{+/+}/M83^{+/-} and APOE ϵ 4^{+/+}/M83^{+/-} mice exhibited significantly higher levels of 2G5 pathology compared to M83^{+/-} mice, however, α Syn Δ C-103 pathology in this region failed to show a significant correlation to days to terminal motor symptoms (Fig. 7b). In the pons, α Syn Δ C-103 immunoreactivity was higher in M83^{+/-} than in APOE ϵ 4^{+/+}/M83^{+/-} mice (Fig. 7c), while, cortical α Syn Δ C-103 positive pathology was highest in APOE ϵ 4^{+/+}/M83^{+/-} mice (Fig. 7d). Interestingly, α Syn Δ C-103 immunoreactivity in the pons and cortex was associated with elongated survival in M83^{+/-}, but not in APOE ϵ 3^{+/+}/M83^{+/-} or APOE ϵ 4^{+/+}/M83^{+/-} (Fig. 7c–d).

Evaluation of α Syn Δ C-114 (1A2) immunostaining revealed moderate positivity in the spine, hindbrain and midbrain and relative few positive inclusions within the forebrain for all cohorts (Fig. 8a). For regions that displayed genotype-specific differences such as the medulla and midbrain, we performed additional statistical analyses (Fig. 8b, c). APOE ϵ 3^{+/+}/M83^{+/-} mice had greater 1A2-positive inclusion pathology in the medulla compared to M83^{+/-} (Fig. 8b) and in the midbrain compared to APOE ϵ 4^{+/+}/M83^{+/-} mice (Fig. 8c). α Syn Δ C-114 immunoreactivity in the medulla but not in the midbrain

(See figure on next page.)

Fig. 6 Regionally dynamic α Syn Δ C immunoreactive pathology is differentially regulated by APOE genotype. The burden of α Syn Δ C positive inclusions in the spinal cord, medulla, pons, midbrain, hypothalamus, thalamus, cortex and striatum of PFF-injected M83^{+/-}, APOE ϵ 4^{+/+}/M83^{+/-} and APOE ϵ 3^{+/+}/M83^{+/-} mice were scored by 3 independent observers. Averaged scores were normalized to 81A (pSer129) and analyzed using 2-way ANOVA and corrected using Tukey's multiple comparisons test. Data represents means \pm SEM. * $p < 0.05$; ** $p < 0.01$; *** $p < 0.001$; **** $p < 0.0001$

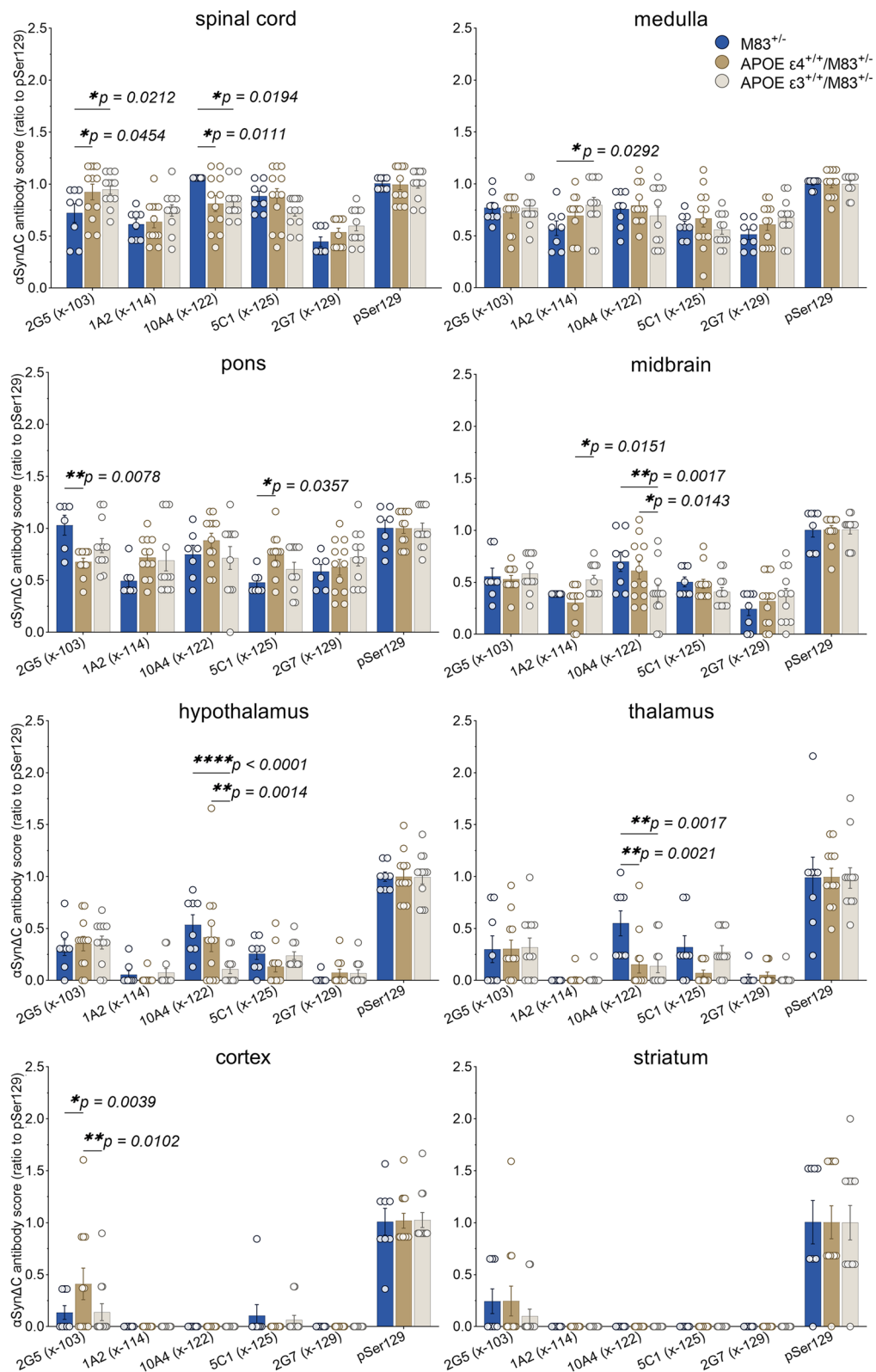


Fig. 6 (See legend on previous page.)

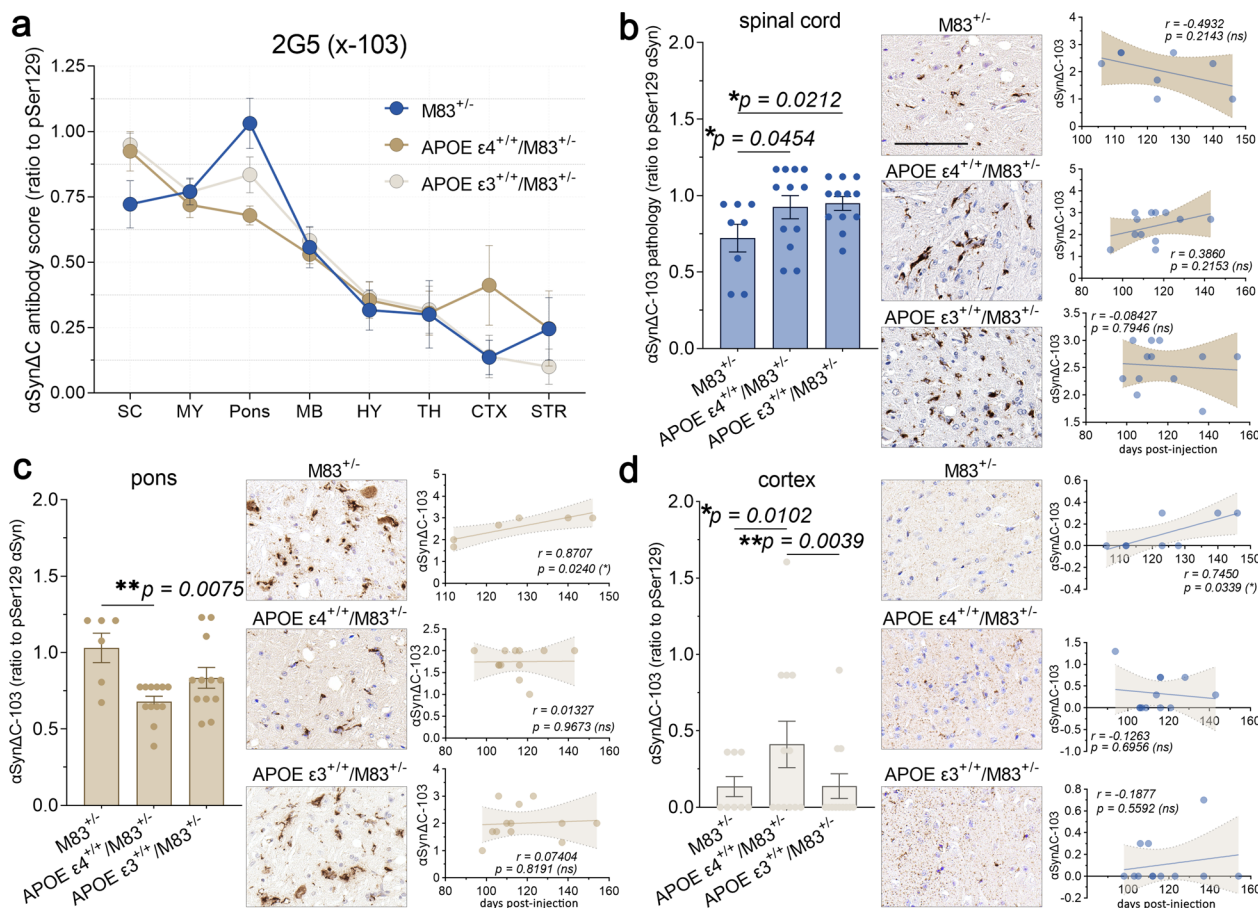


Fig. 7 aSynΔC-103 immunoreactivity in the pons and cortex is associated with survival in time in M83^{+/-} intramuscular injected with PFFs, but not in APOE ε4^{+/-}/M83^{+/-} or APOE ε3^{+/-}/M83^{+/-}. **(a)** Graph summarizing burden of aSynΔC-103 positive inclusions in the spinal cord (SC), medulla (MY), pons, midbrain (MB), hypothalamus (HY), thalamus (TH), cortex (CTX) and striatum (STR) of PFF-injected M83^{+/-}, APOE ε4^{+/-}/M83^{+/-} and APOE ε3^{+/-}/M83^{+/-} mice depicted as mean with SEM. **(b)** Semi-quantification and representative images of aSynΔC-103 immunoreactivity with correlational analysis between spinal aSynΔC-103 immunoreactivity and d.p.i. for each cohort. **(c)** Semi-quantification and representative images of aSynΔC-103 immunoreactivity with correlational analysis between aSynΔC-103 immunoreactivity in the pons and d.p.i. for each cohort. **(d)** Semi-quantification and representative images of aSynΔC-103 immunoreactivity with correlational analysis between aSynΔC-103 immunoreactivity in the cortex and d.p.i. for each cohort. Results were analyzed using 2-way ANOVA and corrected using Tukey's multiple comparisons test; data represent means +/- SEM. Pearson correlation coefficients between aSynΔC-103 positivity and d.p.i. were computed with the assumption that data are sampled from Gaussian distribution. Pearson r and two-tailed p-values are indicated on graph. Simple linear regression is shown with dotted lines depicting 95% confidence intervals. n.s. not significant; *p < 0.05; **p < 0.01; ***p < 0.001; ****p < 0.0001. Scale bar = 100 μm

(See figure on next page.)

Fig. 8 Medullary aSynΔC-114 inclusion pathology is positively correlated with onset of motor symptoms in APOE ε4^{+/-}/M83^{+/-} mice. **(a)** Graph summarizing burden of aSynΔC-114 positive inclusions in the spinal cord (SC), medulla (MY), pons, midbrain (MB), hypothalamus (HY), thalamus (TH), cortex (CTX) and striatum (STR) of PFF-injected M83^{+/-}, APOE ε4^{+/-}/M83^{+/-} and APOE ε3^{+/-}/M83^{+/-} mice depicted as mean with SEM. **(b)** Semi-quantification and representative images of aSynΔC-114 immunoreactivity in the medulla with correlational analysis between aSynΔC-114 immunoreactivity and d.p.i. for each cohort. **(c)** Semi-quantification and representative images of aSynΔC-114 immunoreactivity with correlational analysis between aSynΔC-114 immunoreactivity in the midbrain and d.p.i. for each cohort. M83^{+/-} horizontal line. Results were analyzed using 2-way ANOVA and corrected using Tukey's multiple comparisons test; data represent means +/- SEM. Pearson correlation coefficients between aSynΔC-114 positivity and d.p.i. were computed with the assumption that data are sampled from Gaussian distribution. Pearson r and two-tailed p-values are indicated on graph. Simple linear regression is shown with dotted lines depicting 95% confidence intervals. n.s. not significant; *p < 0.05; **p < 0.01; ***p < 0.001; ****p < 0.0001. Scale bar = 100 μm

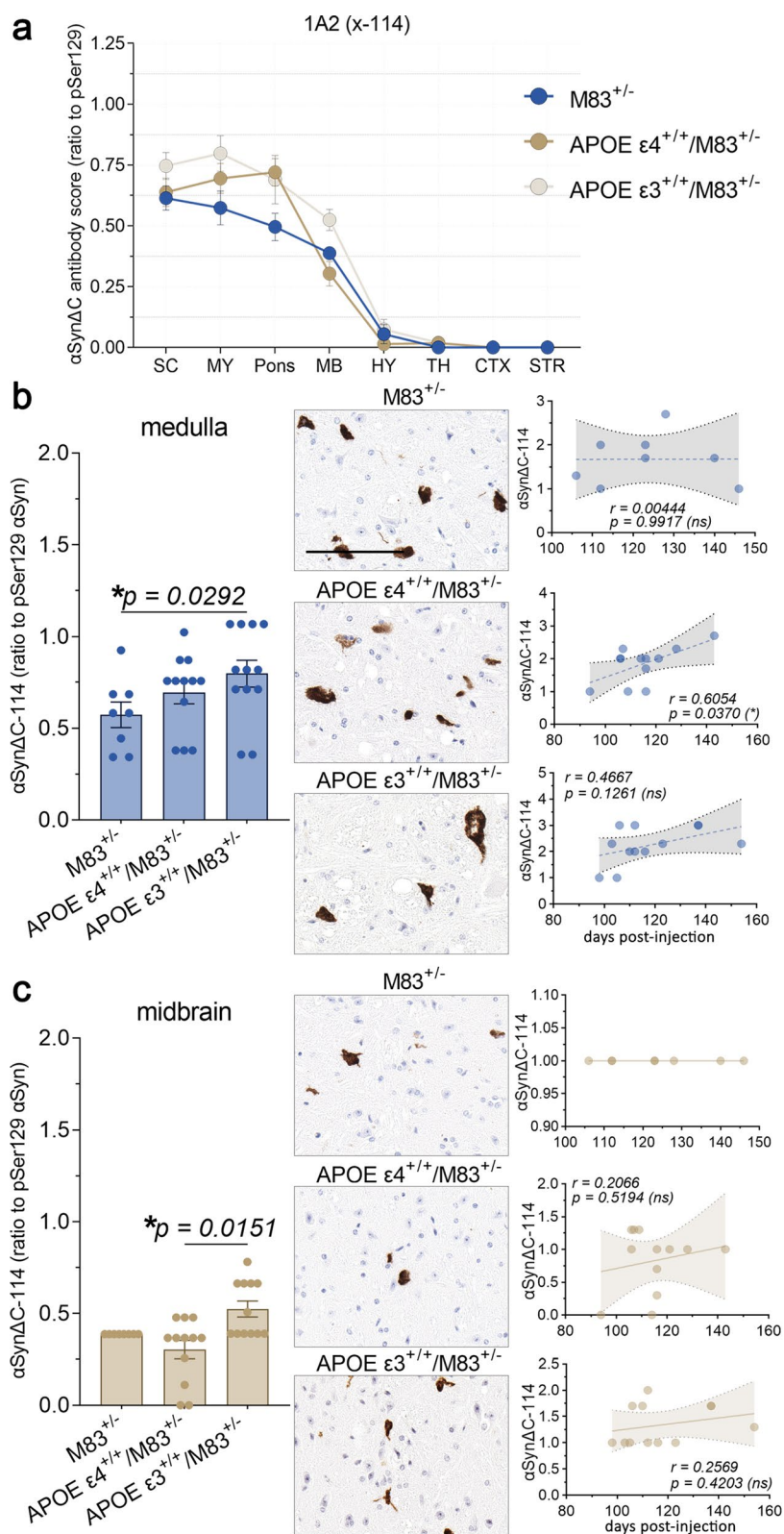


Fig. 8 (See legend on previous page.)

was positively associated with days to terminal motor symptoms in APOE $\epsilon 4^{+/+}/M83^{+/-}$ mice (Fig. 8b, c). There was no association between 1A2-positive inclusion pathology and days to terminal motor symptoms post PFF injection for the other genotypes.

Examination of α Syn Δ C-122 (10A4) immunostaining revealed a higher burden of positive pathology in the spine, hindbrain and midbrain for all cohorts compared to forebrain regions (Fig. 9a). For regions that displayed genotype-specific differences, such as the spinal cord, midbrain, hypothalamus and thalamus, we performed additional statistical analyses (Fig. 9b–e). M83 $^{+/-}$ mice demonstrated a greater burden of 10A4 positive inclusion pathology compared to APOE $\epsilon 3^{+/+}/M83^{+/-}$ and APOE $\epsilon 4^{+/+}/M83^{+/-}$ mice in the spine (Fig. 9b). In the midbrain and hypothalamus, M83 $^{+/-}$ and APOE $\epsilon 4^{+/+}/M83^{+/-}$ mice both exhibited greater levels of α Syn Δ C-122 (10A4) positive immunostaining compared to APOE $\epsilon 3^{+/+}/M83^{+/-}$ mice (Fig. 9c–d). However, in the thalamus, M83 $^{+/-}$ mice again demonstrated a greater burden of 10A4 positive inclusion pathology in comparison to APOE $\epsilon 3^{+/+}/M83^{+/-}$ and APOE $\epsilon 4^{+/+}/M83^{+/-}$ mice (Fig. 9e). Interestingly, thalamic 10A4 positivity in APOE $\epsilon 4^{+/+}/M83^{+/-}$ mice positively correlated with a later onset of motor symptoms.

Analysis of α Syn Δ C-125 (5C1) immunostaining revealed a decreasing trend of positive pathology in all cohorts, as distance from injection site increased (Fig. 10a). Further analysis revealed that APOE $\epsilon 4^{+/+}/M83^{+/-}$ mice exhibited greater pontine 5C1-positive pathology compared to M83 $^{+/-}$ mice, however, there was no correlation with onset of terminal motor symptoms post PFF injection (Fig. 10b). α Syn Δ C-129 (2G7) immunostaining of α Syn pathological inclusions was also more abundant closer to the injection site, including the spine, hindbrain and midbrain compared to forebrain regions (Fig. 6) but there was no statistically significant difference between any of the genotypes injected with PFFs.

Discussion

Our study investigated the spatiotemporal characterization of a series of α Syn Δ C species that occurs during pathogenesis in a peripheral to CNS seeded model of synucleinopathies. This IM seeding model provides the ability to assess changes associated with the processive spatial formation of α Syn pathology along predicted neuroanatomical pathways following the prion-type neuroinvasion of the CNS. Our findings revealed concurrent accumulation of α Syn Δ C with α Syn phosphorylated at pSer129, as well as an APOE isoform-dependent alteration of α Syn Δ C-positive inclusion accumulation (Fig. 11), suggesting that proteolytic processing of α Syn may be a key component to the early stages of pathology and may differentiate stages of disease progression. Our findings show that α Syn Δ C-103, -122 and -125 occur at detectable levels in α Syn aggregates as early as 2 m.p.i. when the formation of α Syn pathology starts, and that by the terminal endpoint, α Syn Δ C-103, -114, -122, -125 and -129 are all observed, at various levels, in pathological inclusions in synaptically connected regions, throughout the neuroaxis (Fig. 11a). Furthermore, we demonstrate that while α Syn-APOE mice develop mature α Syn inclusion pathology and paralysis, at a rate not significantly different from TgM83 $^{+/-}$ controls, the regionality and disposition of α Syn Δ C positive pathology is indeed influenced by the presence of different APOE alleles (Fig. 11b), although the mechanism is unclear. This suggests a role for ApoE isoforms in the regulation of α Syn metabolism; further studies are needed to elaborate upon this relationship.

In this study, we characterized the temporal and spatial accumulation of carboxy-truncated α Syn at specific residues (103, 114, 122, 125, and 129) in the CNS after PFF injection into the hindleg gastrocnemius muscle of different TgM83 $^{+/-}$ -based mouse models. Intramuscular PFF injection is a useful tool for modeling the prion-like spread of seeds through connected neuron populations, as this method of neuroinvasion follows defined groups of neurons in the spinal cord, thereby not confounded by possible dissemination that may occur with intracerebral injections. For spatiotemporal analysis in our time-course study, we

(See figure on next page.)

Fig. 9 α Syn Δ C-122 immunoreactivity is constrained to the spine and brainstem and is significantly lower in APOE $\epsilon 3^{+/+}/M83^{+/-}$ mice compared to M83 $^{+/-}$. **(a)** Graph summarizing burden of α Syn Δ C-122 positive inclusions in the spinal cord (SC), medulla (MY), pons, midbrain (MB), hypothalamus (HY), thalamus (TH), cortex (CTX) and striatum (STR) of PFF-injected M83 $^{+/-}$, APOE $\epsilon 4^{+/+}/M83^{+/-}$ and APOE $\epsilon 3^{+/+}/M83^{+/-}$ mice depicted as mean with SEM. **(b)** Semi-quantification and representative images of α Syn Δ C-122 immunoreactivity with correlational analysis between spinal α Syn Δ C-122 immunoreactivity and d.p.i. for each cohort. **(c)** Semi-quantification and representative images of α Syn Δ C-122 immunoreactivity with correlational analysis between α Syn Δ C-122 immunoreactivity in the midbrain and d.p.i. for each cohort. **(d)** Semi-quantification and representative images of α Syn Δ C-122 immunoreactivity with correlational analysis between α Syn Δ C-122 immunoreactivity in the hypothalamus and d.p.i. for each cohort. **(e)** Semi-quantification and representative images of α Syn Δ C-122 immunoreactivity with correlational analysis between α Syn Δ C-122 immunoreactivity in the thalamus and d.p.i. for each cohort. Results were analyzed using 2-way ANOVA and corrected using Tukey's multiple comparisons test; data represent means \pm SEM. Pearson correlation coefficients between α Syn Δ C positivity and d.p.i. were computed with the assumption that data are sampled from Gaussian distribution. Pearson r and two-tailed p -values are indicated on graph. Simple linear regression is shown with dotted lines depicting 95% confidence intervals. n.s. not significant; * $p < 0.05$; ** $p < 0.01$; *** $p < 0.001$; **** $p < 0.0001$. Scale bar = 100 μ m

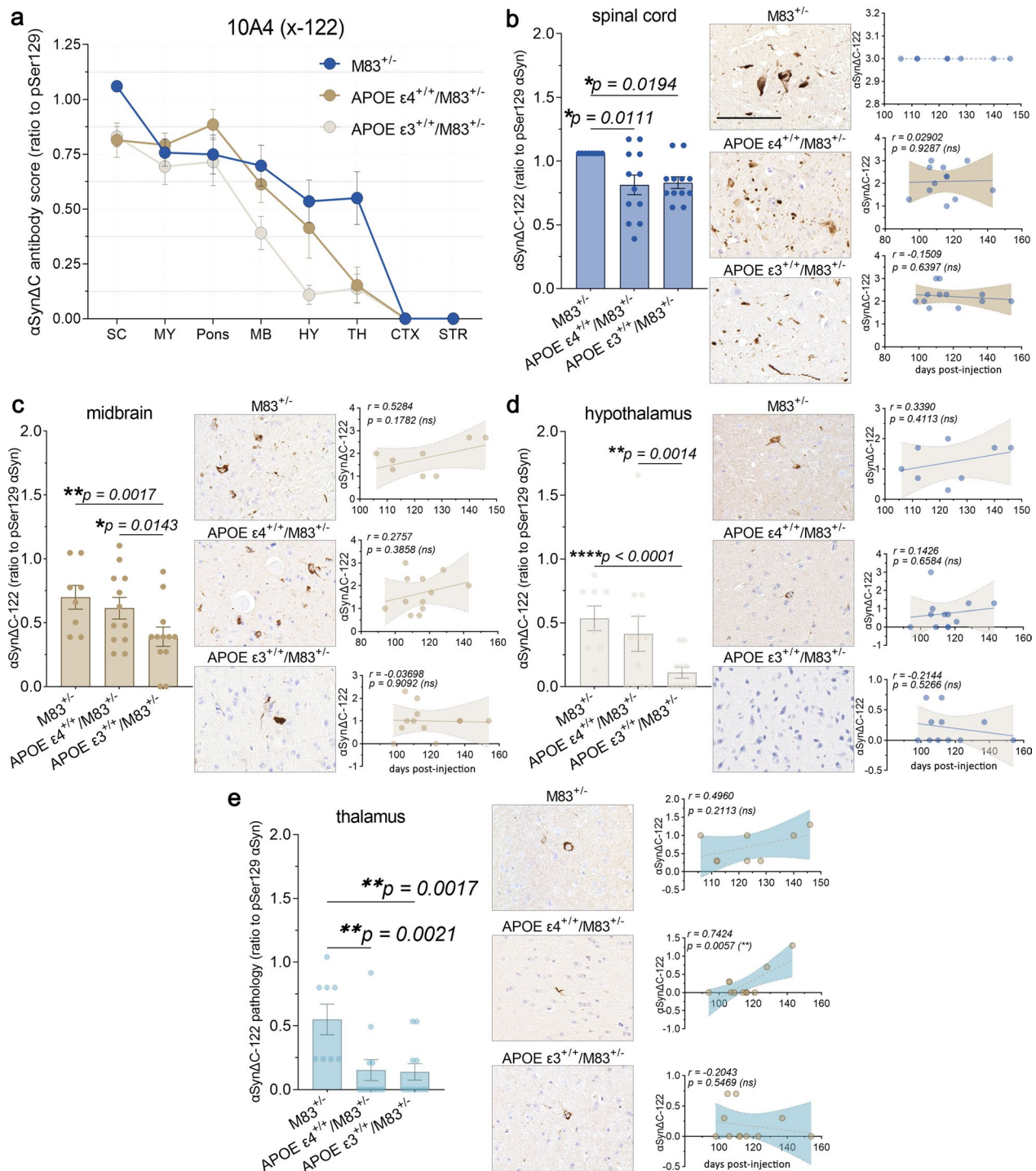


Fig. 9 (See legend on previous page.)

analyzed the mice at 1-, 2-, and 3- months post injection, as well as at terminal stage (approximately 4 months), in regions increasingly distal from injection site. Previously, we have shown the temporal progression of αSyn inclusion pathology in the spine and midbrain by 2 m.p.i., and the ventral thalamus and cortex by 3 m.p.i. Our findings have revealed that

in TgM83^{+/-} mice, with subsequent astroglial and microglial activation [45]. We demonstrated that peripheral PFF injection induced pSer129+αSyn inclusion pathology in the spine and midbrain by 2 m.p.i., and the ventral thalamus and cortex by 3 m.p.i. Our findings have revealed that

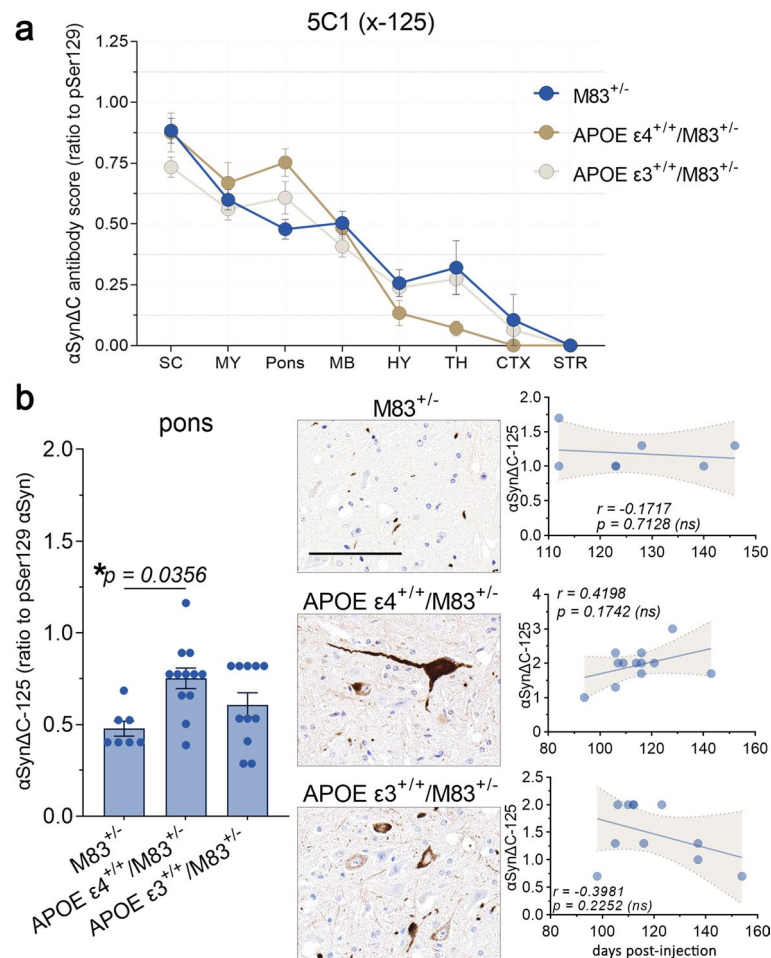


Fig. 10 APOE ϵ 4^{+/-}/M83^{+/-} mice develop a greater burden of α Syn Δ C-125 positive pontine pathology compared to M83^{+/-} mice. **(a)** Graph summarizing burden of α Syn Δ C-125 positive inclusions in the spinal cord (SC), medulla (MY), pons, midbrain (MB), hypothalamus (HY), thalamus (TH), cortex (CTX) and striatum (STR) of intramuscular PFF-injected M83^{+/-}, APOE ϵ 4^{+/-}/M83^{+/-} and APOE ϵ 3^{+/-}/M83^{+/-} mice depicted as mean with SEM. **(b)** Semi-quantification and representative images of α Syn Δ C-125 immunoreactivity with correlational analysis between α Syn Δ C-125 immunoreactivity in the pons and d.p.i. for each cohort. Results were analyzed using 2-way ANOVA and corrected using Tukey's multiple comparisons test; data represent means \pm SEM. Pearson correlation coefficients between α Syn Δ C positivity and d.p.i. were computed with the assumption that data are sampled from Gaussian distribution. Pearson r and two-tailed p -values are indicated on graph. Simple linear regression is shown with dotted lines depicting 95% confidence intervals. n.s. not significant; * $p < 0.05$; ** $p < 0.01$; *** $p < 0.001$; **** $p < 0.0001$. Scale bar = 100 μ m

some forms of α Syn Δ C appear at timepoints concurrent with the onset of pSer129 accumulation, while others are not detected until later timepoints (Fig. 11). We have also shown that α Syn Δ C species progressively accumulate, predominantly in neuroanatomically connected regions, and, by end stage, many reach regions distal from the injection site (Fig. 11). Possible molecular explanations for this include a prion-like mechanism of intercellular spread that is recapitulated in the templated accumulation of α Syn Δ C, wherein truncated species are recruited into fibril assembly. In this model, proteolytic processing of α Syn occurs prior to fibril formation, meaning that aggregate elongation would be dictated by enzymatic activity. Alternatively,

proteolytic degradation of α Syn may occur after fibril formation, where aggregated, full length α Syn proteins are partially degraded by proteases, which remove segments from the C-terminus, exposing the epitopes detected by α Syn Δ C-specific antibodies.

Interestingly, C-truncated α Syn pathology presentation skyrockets in the spine by 3 m.p.i., especially α Syn truncated at residue 103, which is also when we first detected elevated levels of GFAP, cd11b, and Iba1 positivity [45]. These findings suggest that the accumulation of specific α Syn carboxy-truncated species, particularly α Syn Δ C-103, may play a critical role in the rapid stages of prion-like spread of α Syn pathology. Furthermore,

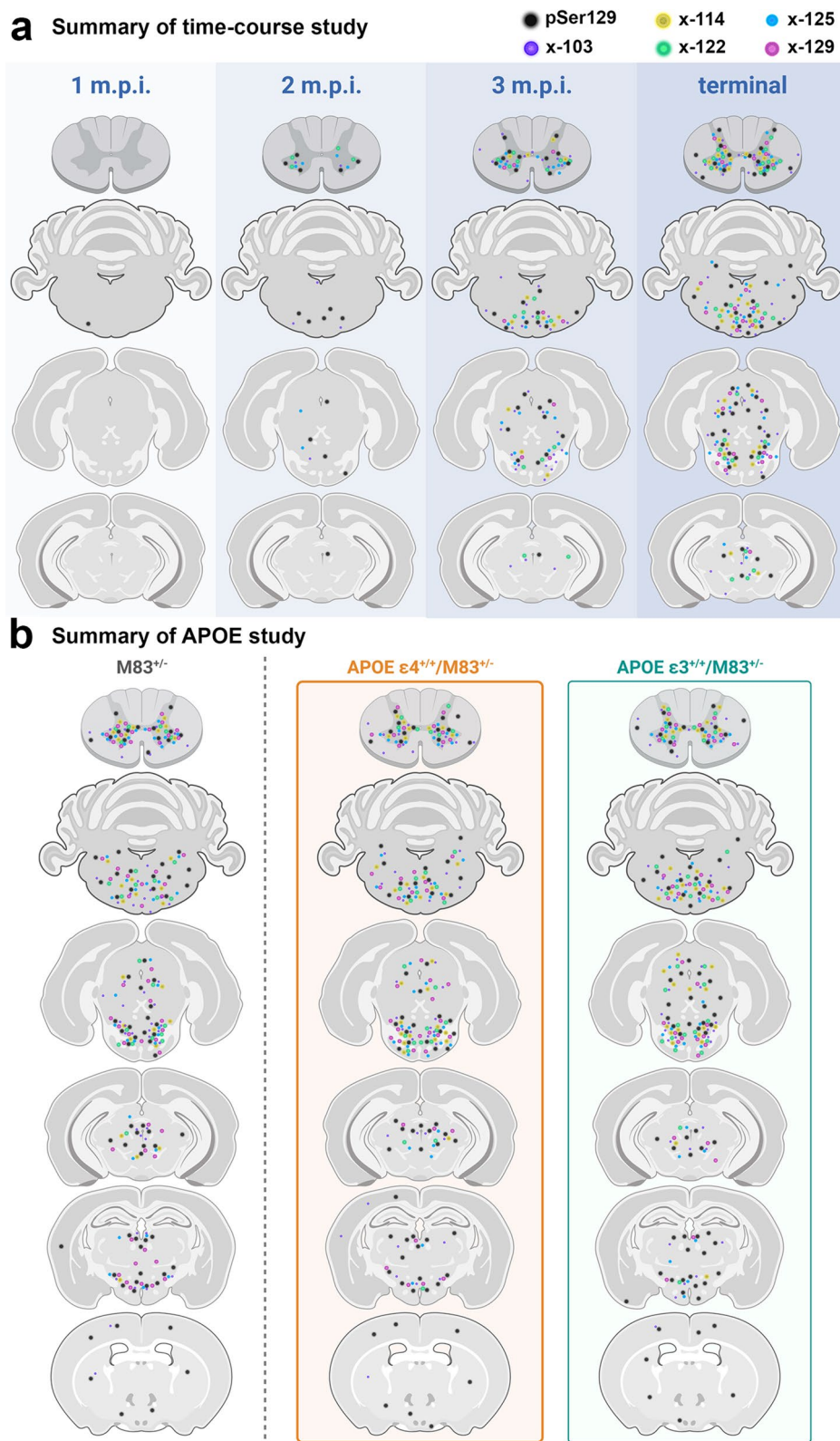


Fig. 11 Schematic summary of the observed pathological findings in various CNS regions, using C-terminally truncated αSyn-specific antibodies. Diagram illustrating data from the (a) time-course study and (b) the APOE study, depicting the relative levels of detected C-terminally truncated αSyn across the neuroaxis. Created with Biorender.com

the temporal and spatial accumulation patterns of α Syn Δ C-103 positive inclusions differ from those of other α Syn Δ C positive inclusions examined in this study, suggesting that proteolysis of α Syn may occur in a specific and regulated manner during the progression of synucleinopathies. Moreover, the fact that the increase in detection of C-terminally truncated α Syn is temporally associated with the occurrence of neuroinflammation indicates that proteolysis may be a contributing factor to the pathogenesis of synucleinopathies by promoting a pro-inflammatory environment. These insights may have important implications for understanding the molecular mechanisms underlying synucleinopathies and developing targeted therapies aimed at preventing or slowing their progression. Future studies will investigate the role of the individual α Syn Δ C species in modulating the initiation and progression of prion-type α Syn pathogenesis and the impact on associated neuroinflammation.

Supplementary Information

The online version contains supplementary material available at <https://doi.org/10.1186/s40478-023-01623-9>.

Additional file 1. Figure S1: Low magnification images depicting accumulation of C-terminally truncated α Syn in the spine of TgM83^{+/-} mice following intramuscular administration of PFFs. Representative IHC images comparing the pathological deposition of α Syn TgM83^{+/-} mice at 1-, 2-, 3- months post injection or terminal stage. Antibodies specific for α Syn phosphorylated at Ser129 (81A) and α Syn truncated at residues 103 (2G5), 114 (1A2), 122 (10A4), 125 (5C1) or 129 (2G7) were used for IHC, as indicated. Sections were counterstained with hematoxylin. Scale bar = 300 μ m. **Figure S2:** Representative images of immunostaining with antibodies specific for α Syn (2H6 and 3H19) and p62/sequestrasome-1. Brains and spinal cord from APOE ϵ 3^{+/+}/M83^{+/-} and APOE ϵ 4^{+/+}/M83^{+/-} mice at end stage following intramuscular injection with PFFs were assessed for markers of mature α Syn inclusion pathology using antibodies directed towards α Syn at the N-terminus (2H6) and C-terminus (3H19), as well as sequestrasome-1 (p62). Sections were counterstained with hematoxylin. Scale bar = 100 μ m. **Figure S3:** α Syn inclusion pathology was not detected in the CNS of PBS-injected APOE ϵ 3^{+/+}/M83^{+/-} and APOE ϵ 4^{+/+}/M83^{+/-} mice. Representative images of immunostaining from the spine and medulla of PBS-injected (a) APOE ϵ 4^{+/+}/M83^{+/-} and (b) APOE ϵ 3^{+/+}/M83^{+/-} mice. Tissue was analyzed with antibodies directed towards α Syn phosphorylated at Ser129 (81A), at the N-terminus (2H6) and C-terminus (3H19), as well as sequestrasome-1 (p62). Sections were counterstained with hematoxylin. Scale bar = 300 μ m.

Acknowledgements

This work was supported by grants from the National Institute of Neurological Disorders and Stroke (R01NS089022, R01NS100876, RF1NS129567, RF1AG057933). G.M.L. was supported by T32NS082168 training grant from National Institute of Neurological Disorders and Stroke. Z.A.S. was supported by fellowship F30AG063446 from the National Institute on Aging.

Author contributions

GML, DB, and BIG designed the experiments. GML, BL, ZAS, SQ, BB, KG, DC, and BIG, performed the experiments. PS and DB provided key experimental resources. GML wrote the manuscript. BIG reviewed and edited manuscript. All authors have read and approved the final manuscript.

Availability of data and materials

The datasets used and analyzed during the current study are available from the corresponding author upon reasonable request.

Declarations

Ethics approval and consent to participate

All procedures were performed according to the National Institute of Health Guide for the Care and Use of Experimental Animals and were approved by the University of Florida Institutional Animal Care and Use Committee.

Competing interests

We declare no competing interest in this manuscript.

Author details

¹Department of Neuroscience, College of Medicine, University of Florida, BMS J483/CTRND, 1275 Center Drive, Gainesville, FL 32610, USA. ²Center for Translational Research in Neurodegenerative Disease, College of Medicine, University of Florida, Gainesville, FL 32610, USA. ³McKnight Brain Institute, College of Medicine, University of Florida, Gainesville, FL 32610, USA. ⁴Department of Medicine, Duke University School of Medicine, Durham, NC, USA.

Received: 31 May 2023 Accepted: 15 July 2023

Published online: 23 July 2023

References

- Allen Institute for Brain Science (2004) Interactive Atlas viewer: Atlas viewer. In: Allen mouse brain atlas. Accessed 13 Mar 2023
- Bassil F, Fernagut PO, Bezard E, Pruvost A, Leste-Lasserre T, Hoang QQ, Ringe D, Petsko GA, Meissner WG (2016) Reducing C-terminal truncation mitigates synucleinopathy and neurodegeneration in a transgenic model of multiple system atrophy. *Proc Natl Acad Sci U S A* 113:9593–9598. <https://doi.org/10.1073/pnas.1609291113>
- Behl T, Kumar S, Althafar ZM, Sehgal A, Singh S, Sharma N, Badavath VN, Yadav S, Bhatia S, Al-Harrasi A, Almohari Y, Almikhlafi MA, Bungau S (2022) Exploring the role of ubiquitin-proteasome system in Parkinson's disease. *Mol Neurobiol* 59:4257–4273. <https://doi.org/10.1007/s12035-022-02851-1>
- Bras J, Guerreiro R, Darwent L, Parkkinen L, Ansorge O, Escott-Price V, Hernandez DG, Nalls MA, Clark LN, Honig LS, Marder K, Van Der Flier WM, Lemstra A, Scheltens P, Roggeva E, St George-Hyslop P, Londos E, Zetterberg H, Ortega-Cubero S, Pastor P, Ferman TJ, Graff-Radford NR, Ross OA, Barber I, Braae A, Brown K, Morgan K, Maetzler W, Berg D, Troakes C, Al-Sarraj S, Lashley T, Compta Y, Revesz T, Lees A, Cairns N, Halliday GM, Mann D, Pickering-Brown S, Dickson DW, Singleton A, Hardy J (2014) Genetic analysis implicates APOE, SNCA and suggests lysosomal dysfunction in the etiology of dementia with Lewy bodies. *Hum Mol Genet* 23:6139–6146. <https://doi.org/10.1093/hmg/ddu334>
- Burré J, Sharma M, Südhof TC (2018) Cell biology and pathophysiology of α -synuclein. *Cold Spring Harb Perspect Med* 8:a024091. <https://doi.org/10.1101/cshperspect.a024091>
- Chen L, Thiruchelvam MJ, Madura K, Richfield EK (2006) Proteasome dysfunction in aged human α -synuclein transgenic mice. *Neurobiol Dis* 23:120–126. <https://doi.org/10.1016/j.nbd.2006.02.004>
- Crystal AS, Giasson BI, Crowe A, Kung MP, Zhuang ZP, Trojanowski JQ, Lee VMY (2003) A comparison of amyloid fibrillogenesis using the novel fluorescent compound K114. *J Neurochem* 86:1359–1368. <https://doi.org/10.1046/j.1471-4159.2003.01949.x>
- Daigle TL, Madisen L, Hage TA, Valley MT, Knoblich U, Larsen RS, Takeno MM, Huang L, Gu H, Larsen R, Mills M, Bosma-Moody A, Siverts LA, Walker M, Graybuck LT, Yao Z, Fong O, Nguyen TN, Garren E, Lenz GH, Chavarha M, Pendergraft J, Harrington J, Hirokawa KE, Harris JA, Nicovich PR, McGraw MJ, Ollerenshaw DR, Smith KA, Baker CA, Ting JT, Sunkin SM, Lecoq J, Lin MZ, Boyden ES, Murphy GJ, da Costa NM, Waters J, Li L, Tasic B, Zeng H (2018) A suite of transgenic driver and reporter mouse lines with enhanced brain-cell-type targeting and

- functionality. *Cell* 174:465–480.e22. <https://doi.org/10.1016/j.cell.2018.06.035>
9. Davis AA, Inman CE, Wargel ZM, Dube U, Freeberg BM, Galluppi A, Haines JN, Dhavale DD, Miller R, Choudhury FA, Sullivan PM, Cruchaga C, Perlmuter JS, Ulrich JD, Benitez BA, Kotzbauer PT, Holtzman DM (2020) APOE genotype regulates pathology and disease progression in synucleinopathy. *Sci Transl Med* 12:eay3069. <https://doi.org/10.1126/scitranslmed.aay3069>
 10. Dhillon J-KS, Riffe C, Moore BD, Ran Y, Chakrabarty P, Golde TE, Giasson BI (2017) A novel panel of α -synuclein antibodies reveal distinctive staining profiles in synucleinopathies. *PLoS ONE* 12:e0184731. <https://doi.org/10.1371/journal.pone.0184731>
 11. Dickson DW, Heckman MG, Murray ME, Soto AI, Walton RL, Diehl NN, van Gerpen JA, Uitti RJ, Wszolek ZK, Ertekin-Taner N, Knopman DS, Petersen RC, Graff-Radford NR, Boeve BF, Bu G, Ferman TJ, Ross OA (2018) APOE $\epsilon 4$ is associated with severity of Lewy body pathology independent of Alzheimer pathology. *Neurology* 91:e1182–e1195. <https://doi.org/10.1212/WNL.00000000000006212>
 12. Dikic I (2017) Proteasomal and autophagic degradation systems. *Annu Rev Biochem* 86:193–224. <https://doi.org/10.1146/annurev-biochem-061516-044908>
 13. Duda JE, Giasson BI, Gur TL, Montine TJ, Robertson D, Biaggioni I, Hurtig HI, Stern MB, Gollomp SM, Grossman M, Lee VMY, Trojanowski JQ (2000) Immunohistochemical and biochemical studies demonstrate a distinct profile of α -Synuclein permutations in multiple system atrophy. *J Neuro-pathol Exp Neurol* 59:830–841. <https://doi.org/10.1093/jnen/59.9.830>
 14. Gallardo G, Schlüter OM, Südhof TC (2008) A molecular pathway of neurodegeneration linking α -synuclein to ApoE and A β peptides. *Nat Neurosci* 11:301–308. <https://doi.org/10.1038/nn2058>
 15. Giasson BI, Lee VMY (2003) Are ubiquitination pathways central to parkinson's disease? *Cell* 114:1–8. [https://doi.org/10.1016/S0092-8674\(03\)00509-9](https://doi.org/10.1016/S0092-8674(03)00509-9)
 16. Goedert M, Jakes R, Spillantini MG (2017) The synucleinopathies: twenty years on. *J Parkinsons Dis* 7:S51–S69. <https://doi.org/10.3233/JPD-179005>
 17. Grassi D, Howard S, Zhou M, Diaz-Perez N, Urban NT, Guerrero-Given D, Kamasawa N, Volpicelli-Daley LA, LoGrasso P, Lasmézas CI (2018) Identification of a highly neurotoxic α -synuclein species inducing mitochondrial damage and mitophagy in Parkinson's disease. *Proc Natl Acad Sci U S A* 115:E2634–E2643. <https://doi.org/10.1073/pnas.1713849115>
 18. Guerreiro R, Ross OA, Kun-Rodrigues C, Hernandez DG, Orme T, Eicher JD, Shepherd CE, Parkkinen L, Darwent L, Heckman MG, Scholz SW, Troncoso JC, Pletnikova O, Ansorge O, Clarimon J, Lleo A, Morenas-Rodríguez E, Clark L, Honig LS, Marder K, Lemstra A, Rogava E, St George-Hyslop P, Londo E, Zetterberg H, Barber I, Braae A, Brown K, Morgan K, Troakes C, Al-Sarraj S, Lashley T, Holton J, Compta Y, Van Deerlin V, Serrano GE, Beach TG, Lesage S, Galasko D, Masliah E, Santana I, Pastor P, Diez-Fairen M, Aguilar M, Tienari PJ, Myllylkangas L, Oinas M, Revesz T, Lees A, Boeve BF, Petersen RC, Ferman TJ, Escott-Price V, Graff-Radford N, Cairns NJ, Morris JC, Pickering-Brown S, Mann D, Halliday GM, Hardy J, Trojanowski JQ, Dickson DW, Singleton A, Stone DJ, Bras J (2018) Investigating the genetic architecture of dementia with Lewy bodies: a two-stage genome-wide association study. *Lancet Neurol* 17:64–74. [https://doi.org/10.1016/S1474-4422\(17\)30400-3](https://doi.org/10.1016/S1474-4422(17)30400-3)
 19. Harris JA, Mihalas S, Hirokawa KE, Whitesell JD, Choi H, Bernard A, Bohn P, Caldejon S, Casal L, Cho A, Feiner A, Feng D, Gaudreault N, Gerfen CR, Graddis N, Groblewski PA, Henry AM, Ho A, Howard R, Knox JE, Kuan L, Kuang X, Lecoq J, Lesnar P, Li Y, Luviano J, McConoughey S, Mortrud MT, Naeemi M, Ng L, Oh SW, Ouellette B, Shen E, Sorensen SA, Wakeman W, Wang Q, Wang Y, Williford A, Phillips JW, Jones AR, Koch C, Zeng H (2019) Hierarchical organization of cortical and thalamic connectivity. *Nature* 575:195–202. <https://doi.org/10.1038/s41586-019-1716-z>
 20. Hass EW, Sorrentino ZA, Xia Y, Lloyd GM, Trojanowski JQ, Prokop S, Giasson BI (2021) Disease-, region- and cell type specific diversity of α -synuclein carboxy terminal truncations in synucleinopathies. *Acta Neuropathol Commun* 9:146. <https://doi.org/10.1186/s40478-021-01242-2>
 21. Huang X, Chen P, Kaufer DI, Tröster AI, Poole C (2006) Apolipoprotein E and dementia in Parkinson disease: A meta-analysis. *Arch Neurol* 63:189–193
 22. Jin Y, Li F, Sonoustoun B, Kondru NC, Martens YA, Qiao W, Heckman MG, Ikezu TC, Li Z, Burgess JD, Amerna D, O'Leary J, DeTure MA, Zhao J, McLean PJ, Dickson DW, Ross OA, Bu G, Zhao N (2022) APOE4 exacerbates α -synuclein seeding activity and contributes to neurotoxicity in Alzheimer's disease with Lewy body pathology. *Acta Neuropathol* 143:641–662. <https://doi.org/10.1007/s00401-022-02421-8>
 23. Knouff C, Hinsdale ME, Mezdour H, Altenburg MK, Watanabe M, Quarfordt SH, Sullivan PM, Maeda N (1999) Apo E structure determines VLDL clearance and atherosclerosis risk in mice. *J Clin Invest* 103:1579–1586. <https://doi.org/10.1172/JCI6172>
 24. Kuusisto E, Parkkinen L, Alafuzoff I (2003) Morphogenesis of Lewy Bodies: Dissimilar Incorporation of α -Synuclein, Ubiquitin, and p62. *J Neuropathol Exp Neurol* 62:1241–1253. <https://doi.org/10.1093/jnen/62.12.1241>
 25. Lashuel HA, Mahul-Mellier A-L, Novello S, Hegde RN, Jasiqi Y, Altay MF, Donzelli S, DeGuire SM, Burai R, Magalhães P, Chiki A, Ricci J, Boussouf M, Sadek A, Stoops E, Iseli C, Guex N (2022) Revisiting the specificity and ability of phospho-S129 antibodies to capture alpha-synuclein biochemical and pathological diversity. *npj Park Dis* 8:136. <https://doi.org/10.1038/s41531-022-00388-7>
 26. Lein ES, Hawrylycz MJ, Ao N, Ayres M, Bensinger A, Bernard A, Boe AF, Boguski MS, Brockway KS, Byrnes EJ, Chen L, Chen L, Chen TM, Chin MC, Chong J, Crook BE, Czaplinska A, Dang CN, Datta S, Dee NR, Desaki AL, Desta T, Diep E, Dolbeare TA, Donelan MJ, Dong HW, Dougherty JG, Duncan BJ, Ebbert AJ, Eichele G, Estlin LK, Faber C, Facer BA, Fields R, Fischer SR, Fliiss TP, Frensley C, Gates SN, Glattfelder KJ, Halverson KR, Hart MR, Hohmann JG, Howell MP, Jeung DP, Johnson RA, Karr PT, Kawal R, Kidney JM, Knapiak RH, Kuan CL, Lake JH, Laramee AR, Larsen KD, Lau C, Lemon TA, Liang AJ, Liu Y, Luong LT, Michaels J, Morgan JJ, Morgan RJ, Mortrud MT, Mosqueda NF, Ng LL, Ng R, Orta GJ, Overly CC, Pak TH, Parry SE, Pathak SD, Pearson OC, Puchalski RB, Riley ZL, Rockett HR, Rowland SA, Royall JJ, Ruiz MJ, Sarno NR, Schaffnit K, Shapovalova NV, Sivasay T, Slaughterbeck CR, Smith SC, Smith KA, Smith BI, Sotd AJ, Stewart NN, Stumpf KR, Sunkin SM, Sutram M, Tam A, Teemer CD, Thaller C, Thompson CL, Varnam LR, Visel A, Whitlock RM, Wahnoutka PE, Wolke CK, Wong VY, Wood M, Yaylaoglu MB, Young RC, Youngstrom BL, Yuan XF, Zhang B, Zwingman TA, Jones AR (2007) Genome-wide atlas of gene expression in the adult mouse brain. *Nature* 445:168–176. <https://doi.org/10.1038/nature05453>
 27. Liu B, Ruan J, Chen M, Li Z, Manjengwa G, Schlüter D, Song W, Wang X (2022) Deubiquitinating enzymes (DUBs): decipher underlying basis of neurodegenerative diseases. *Mol Psychiatry* 27:259–268. <https://doi.org/10.1038/s41380-021-01233-8>
 28. Liu CW, Giasson BI, Lewis KA, Lee VM, DeMartino GN, Thomas PJ (2005) A precipitating role for truncated α -synuclein and the proteasome in α -synuclein aggregation: Implications for pathogenesis of parkinson disease. *J Biol Chem* 280:22670–22678. <https://doi.org/10.1074/jbc.M501508200>
 29. Lloyd GM, Sorrentino ZA, Quintin S, Gorion K-MM, Bell BM, Paterno G, Long B, Prokop S, Giasson BI (2022) Unique seeding profiles and prion-like propagation of synucleinopathies are highly dependent on the host in human α -synuclein transgenic mice. *Acta Neuropathol* 143:663–685. <https://doi.org/10.1007/s00401-022-02425-4>
 30. Mata IF, Leverenz JB, Weintraub D, Trojanowski JQ, Hurtig HI, Van Deerlin VM, Ritz B, Rausch R, Rhodes SL, Factor SA, Wood-Siverio C, Quinn JF, Chung KA, Peterson AL, Espay AJ, Revilla FJ, Devoto J, Hu SC, Cholerton BA, Wan JY, Montine TJ, Edwards KL, Zabetian CP (2014) APOE, MAPT, and SNCA genes and cognitive performance in Parkinson disease. *JAMA Neurol* 71:1405–1412. <https://doi.org/10.1001/jamaneurol.2014.1455>
 31. McKeith IG, Boeve BF, Dickson DW, Halliday G, Taylor JP, Weintraub D, Aarsland D, Galvin J, Attems J, Ballard CG, Bayston A, Beach TG, Blanc F, Bohnen N, Bonanni L, Bras J, Brundin P, Burn D, Chen-Plotkin A, Duda JE, El-Agnaf O, Feldman H, Ferman TJ, Ffytche D, Fujishiro H, Galasko D, Goldman JG, Gomperts SN, Graff-Radford NR, Honig LS, Iranzo A, Kantarci K, Kaufer D, Kukull W, Lee VMY, Leverenz JB, Lewis S, Lipka C, Lunde A, Masellis M, Masliah E, McLean P, Mollenhauer B, Montine TJ, Moreno E, Mori E, Murray M, O'Brien JT, Orimo S, Postuma RB, Ramaswamy S, Ross OA, Salmon DP, Singleton A, Taylor A, Thomas A, Tiraboschi P, Toledo JB, Trojanowski JQ, Tsuang D, Walker Z, Yamada M, Kosaka K (2017) Diagnosis and management of dementia with Lewy bodies. *Neurology* 89:88–100
 32. Nonaka T, Iwatsubo T, Hasegawa M (2005) Ubiquitination of α -synuclein. *Biochemistry* 44:361–368. <https://doi.org/10.1021/bi0485528>
 33. Oh SW, Harris JA, Ng L, Winslow B, Cain N, Mihalas S, Wang Q, Lau C, Kuan L, Henry AM, Mortrud MT, Ouellette B, Nguyen TN, Sorensen SA, Slaughterbeck CR, Wakeman W, Li Y, Feng D, Ho A, Nicholas E, Hirokawa KE, Bohn P, Joines KM, Peng H, Hawrylycz MJ, Phillips JW, Hohmann JG, Wahnoutka

- P, Gerfen CR, Koch C, Bernard A, Dang C, Jones AR, Zeng H (2014) A mesoscale connectome of the mouse brain. *Nature* 508:207–214. <https://doi.org/10.1038/nature13186>
34. Okubadejo NU, Okunoye O, Ojo OO, Arabambi B, Akinyemi RO, Osagigbovo GO, Abubakar SA, Iwuozo EU, Wahab KW, Agabi OP, Agulanna U, Imarihiagbe FA, Abiodun OV, Achoru CO, Adebowale AA, Adeniji O, Akpekpe JE, Ali MW, Ani-Oshoku I, Arigbodi O, Balarabe SA, Bello AH, Ekenze OS, Erameh CO, Farombi TH, Fawale MB, Komolafe MA, Nwani PO, Nwazor EO, Nyandaiti Y, Obehighe EE, Obiabo YO, Odeniyi OA, Odiase FE, Ojini FI, Onwuegbuzie GA, Osemwegie N, Oshinaike OO, Otubogun FM, Oyakhire SI, Taiwo FT, Williams UE, Ozomma S, Zubair Y, Hernandez D, Bandres-Ciga S, Blauwendraat C, Singleton A, Houlden H, Hardy J, Rzig M (2022) APOE E4 is associated with impaired self-declared cognition but not disease risk or age of onset in Nigerians with Parkinson's disease. *npj Park Dis* 8:155. <https://doi.org/10.1038/s41531-022-00411-x>
 35. Outeiro TF, Alcalay RN, Antonini A, Attems J, Bonifati V, Cardoso F, Cheseselet M-F, Hardy J, Madeo G, McKeith I, Mollenhauer B, Moore DJ, Rascol O, Schlossmacher MG, Soreq H, Stefanis L, Ferreira JJ (2023) Defining the riddle in order to solve it: there is more than one "Parkinson's disease." *Mov Disord Epub ahead*. <https://doi.org/10.1002/mds.29419>
 36. Outeiro TF, Koss DJ, Erskine D, Walker L, Kurzawa-Akanbi M, Burn D, Donaghy P, Morris C, Taylor JP, Thomas A, Attems J, McKeith I (2019) Dementia with Lewy bodies: an update and outlook. *Mol Neurodegener* 14:5. <https://doi.org/10.1186/s13024-019-0306-8>
 37. Paul KC, Rausch R, Creek MM, Sinsheimer JS, Bronstein JM, Bordelon Y, Ritz B (2016) APOE, MAPT, and COMT and Parkinson's disease susceptibility and cognitive symptom progression. *J Parkinsons Dis* 6:349–359. <https://doi.org/10.3233/JPD-150762>
 38. Payami H, Nutt J, Kaye J, Bird T, Camicioli R, Zarepari S, Sexton G, Swanson P (2002) Age at onset of Parkinson disease and apolipoprotein E genotypes. *Am J Med Genet* 107:156–161. <https://doi.org/10.1002/ajmg.10111>
 39. Pu JL, Jin CY, Wang ZX, Fang Y, Li YL, Xue NJ, Zheng R, Lin ZH, Yan YQ, Si XL, Chen Y, Liu Y, Song Z, Yan YP, Tian J, Yin XZ, Zhang BR (2022) Apolipoprotein E genotype contributes to motor progression in Parkinson's disease. *Mov Disord* 37:196–200. <https://doi.org/10.1002/mds.28805>
 40. Quintin S, Lloyd GM, Paterno G, Xia Y, Sorrentino Z, Bell BM, Gorion K-M, Lee EB, Prokop S, Giasson BI (2023) Cellular processing of α -synuclein fibrils results in distinct physiological C-terminal truncations with a major cleavage site at residue Glu 114. *J Biol Chem* 299:104912. <https://doi.org/10.1016/j.jbc.2023.104912>
 41. Rongve A, Witoelar A, Ruiz A, Athanasios L, Abdelnour C, Clarimon J, Heilmann-Heimbach S, Hernández I, Moreno-Grau S, de Rojas I, Morenas-Rodríguez E, Fladby T, Sando SB, Bråthen G, Blanc F, Bousiges O, Lemstra AW, van Steenoven I, Londos E, Almdahl IS, Pålhaugen L, Eriksen JA, Djurovic S, Stordal E, Saltvedt I, Ulstein ID, Bettella F, Desikan RS, Idland AV, Toft M, Pihlstrøm L, Snaedal J, Tárrega L, Boada M, Lleó A, Stefánsson H, Stefánsson K, Ramírez A, Aarsland D, Andreassen OA (2019) GBA and APOE ϵ 4 associate with sporadic dementia with Lewy bodies in European genome wide association study. *Sci Rep* 9:7013. <https://doi.org/10.1038/s41598-019-43458-2>
 42. Sacino AN, Brooks M, Thomas MA, McKinney AB, Lee S, Regenhart RW, McGarvey NH, Ayers JL, Notterpek L, Borchelt DR, Golde TE, Giasson BI (2014) Intramuscular injection of α -synuclein induces CNS α -synuclein pathology and a rapid-onset motor phenotype in transgenic mice. *Proc Natl Acad Sci* 111:10732–10737. <https://doi.org/10.1073/pnas.1321785111>
 43. Sorrentino ZA, Brooks MMT, Hudson V, Rutherford NJ, Golde TE, Giasson BI, Chakrabarty P (2017) Intrastratial injection of α -synuclein can lead to widespread synucleinopathy independent of neuroanatomic connectivity. *Mol Neurodegener* 12:40. <https://doi.org/10.1186/s13024-017-0182-z>
 44. Sorrentino ZA, Giasson BI (2020) The emerging role of α -synuclein truncation in aggregation and disease. *J Biol Chem* 295:10224–10244. <https://doi.org/10.1074/jbc.REV120.011743>
 45. Sorrentino ZA, Xia Y, Funk C, Riffe CJ, Rutherford NJ, Ceballos Diaz C, Sacino AN, Price ND, Golde TE, Giasson BI, Chakrabarty P (2018) Motor neuron loss and neuroinflammation in a model of α -synuclein-induced neurodegeneration. *Neurobiol Dis* 120:98–106. <https://doi.org/10.1016/j.nbd.2018.09.005>
 46. Sullivan PM, Mezdour H, Aratani Y, Knouff C, Najib J, Reddick RL, Quarfordt SH, Maeda N (1997) Targeted replacement of the mouse apolipoprotein E gene with the common human APOE3 allele enhances diet-induced hypercholesterolemia and atherosclerosis. *J Biol Chem* 272:17972–17980. <https://doi.org/10.1074/jbc.272.29.17972>
 47. Sullivan PM, Mezdour H, Quarfordt SH, Maeda N (1998) Type III hyperlipoproteinemia and spontaneous atherosclerosis in mice resulting from gene replacement of mouse Apoe with human APOE*2. *J Clin Invest* 102:130–135. <https://doi.org/10.1172/JCI2673>
 48. Szewdo AA, Dalen I, Pedersen KF, Camacho M, Bäckström D, Forsgren L, Tzoulis C, Winder-Rhodes S, Hudson G, Liu G, Scherzer CR, Lawson RA, Yarnall AJ, Williams-Gray CH, Macleod AD, Counsell CE, Tysnes OB, Alves G, Maple-Grødem J (2022) GBA and APOE impact cognitive decline in Parkinson's disease: a 10-year population-based study. *Mov Disord* 37:1016–1027. <https://doi.org/10.1002/mds.28932>
 49. Tsuang D, Leverenz JB, Lopez OL, Hamilton RL, Bennett DA, Schneider JA, Buchman AS, Larson EB, Crane PK, Kaye JA, Kramer P, Woltjer R, Trojanowski JQ, Weintraub D, Chen-Plotkin AS, Irwin DJ, Rick J, Schellenberg GD, Watson GS, Kukull W, Nelson PT, Jicha GA, Neltner JH, Galasko D, Masliah E, Quinn JF, Chung KA, Yearout D, Mata IF, Wan JY, Edwards KL, Montine TJ, Zabetian CP (2013) APOE ϵ 4 increases risk for dementia in pure synucleinopathies. *JAMA Neurol* 70:223–228. <https://doi.org/10.1001/jama.neuro.2013.600>
 50. Waxman EA, Giasson BI (2008) Specificity and regulation of casein kinase-mediated phosphorylation of alpha-synuclein. *J Neuropathol Exp Neurol* 67:402–416. <https://doi.org/10.1097/NEN.0b013e31816fc995>
 51. Wilhelmus MMM, Bol JGJM, Van Haastert ES, Rozemuller AJM, Bu G, Drukarch B, Hoozemans JJM (2011) Apolipoprotein e and LRP1 increase early in Parkinson's disease pathogenesis. *Am J Pathol* 179:2152–2156. <https://doi.org/10.1016/j.ajpath.2011.07.021>
 52. Zhao N, Attrebi ON, Ren Y, Qiao W, Sonustun B, Martens YA, Meneses AD, Li F, Shue F, Zheng J, Van Ingelgom AJ, Davis MD, Kurti A, Knight JA, Linares C, Chen Y, Delenclos M, Liu C-C, Fryer JD, Asmann YW, McLean PJ, Dickson DW, Ross OA, Bu G (2020) APOE4 exacerbates α -synuclein pathology and related toxicity independent of amyloid. *Sci Transl Med* 12:eay1809. <https://doi.org/10.1126/scitranslmed.aay1809>

Publisher's Note

Springer Nature remains neutral with regard to jurisdictional claims in published maps and institutional affiliations.

Ready to submit your research? Choose BMC and benefit from:

- fast, convenient online submission
- thorough peer review by experienced researchers in your field
- rapid publication on acceptance
- support for research data, including large and complex data types
- gold Open Access which fosters wider collaboration and increased citations
- maximum visibility for your research: over 100M website views per year

At BMC, research is always in progress.

Learn more biomedcentral.com/submissions

